



GEORG-AUGUST-UNIVERSITÄT
GÖTTINGEN

Fakultät für
Physik 

Bachelor's Thesis

Signal- und Untergrundstudien am Top-Antitop-Zerfall mit einem Kinematischen Likelihood Fitter

Signal and Background Studies of Top-Antitop Decay with a Kinematic Likelihood Fitter

prepared by

Sven Ebert

from Hildesheim

at the II. Institute of Physics

Thesis period: April 12, 2010 until July 19, 2010

Thesis number: II. Physik-UniGö-BSc-2010/01

Supervisor: Dr. Kevin Kröniger
Dipl.-Phys. Johannes Erdmann

First referee: Prof. Dr. Arnulf Quadt

Second referee: Prof. Dr. Ariane Frey

Zusammenfassung

In dieser Bachelorarbeit wird das Verhalten des Signals und ausgewählter Untergrundprozesse des Top-Antitop-Zerfalls, nach der Rekonstruktion mit einem Kinematischen Likelihood Fitter (KLFitter), untersucht. Dazu werden Monte Carlo generierte $t\bar{t}$ -Ereignisse (Signal) und W +jets-Ereignisse (Untergrund) mit dem Programm KLFitter unter der Annahme, dass diese Signal enthalten, mit einem Maximum Likelihood Ansatz rekonstruiert. Es wird gezeigt, dass nach der Rekonstruktion die Untergrundereignisse immer noch vom Signal unterscheidbar sind, obwohl diese Fitting Prozedur dem Untergrund die Topologie des Signals aufprägt. Eine Anzahl Untergrund diskriminierender Variablen wird studiert, mit dem Ergebnis, dass die Variable $\log L$ die größte diskriminierende Wirkung verspricht.

Außerdem wird gezeigt, dass der KLFitter semileptonische $t\bar{t}$ -Zerfälle mit einem Myon oder einem Elektron im Endzustand in gleicher Weise rekonstruiert. Im letzten Abschnitt wird das Verhalten des KLFitter unter zwei verschiedenen Mengen von Transferfunktionen untersucht.

Abstract

This bachelor thesis presents the studies of top pair reconstructions in the presence of background processes, when reconstructed by a Kinematic Likelihood Fitter (KLFitter). Monte Carlo generated $t\bar{t}$ -events (signal) and W +jets (background) are fitted with the program KLFitter, using the Maximum Likelihood method. It is shown that the background is still distinguishable from the signal after the fit, although the fitting procedure implies the signal topology also for the background events. A set of background discriminating variables is studied, with the outcome that the variable $\log L$ is the most promising one.

It is also shown that the performance of the fitting program to reconstruct semileptonic $t\bar{t}$ -decays with a muon or an electron in the final state is equal. In a last step the behaviour of the KLFitter with two different sets of transfer functions is studied.

Contents

1. Introduction	1
2. The Top Quark in the Standard Model	3
2.1. Particle Interactions	3
2.2. CKM Matrix	6
2.3. Top Quark	7
2.3.1. Top Quark Pair Production	7
2.3.2. Single Top Production	8
2.3.3. Top Decay Topology of Top Quark Pairs	9
2.3.4. Tau Leptons in the Final State	11
2.4. Background Processes to Top-Antitop Decay	11
3. Atlas Detector	13
4. Kinematic Fitting	15
4.1. Maximum Likelihood Method	15
4.2. The Kinematic Likelihood Fitter (KLFitter)	16
4.2.1. Jet-to-Quark Mapping	18
4.2.2. Event Selection	18
4.2.3. In- and Output of the KLFitter	19
4.3. Transfer Functions	20
5. Fitting $\mu\text{on}+\text{jets}$ Final States	21
6. Fitting Background	27
6.1. Used MC Samples	27
6.2. Signal and Background without Selection	27
6.3. Effect of the Event Selection	29

Contents

6.4. Background Discriminating Variables	30
6.4.1. ROC-Curves	33
6.4.2. Correlation between different Variables	34
6.4.3. Exemplary Cuts	35
6.5. Fitting five Jets	42
7. Comparison of two Sets of Transfer Functions	47
8. Conclusion	51
8.1. Outlook	52
9. Appendix	53
A. Fitting muon+jets Final States	53
B. Cuts on Wjets Sample	56
C. Comparison of two Sets of Transfer Functions on e+jets Sample . . .	57

1. Introduction

Elementary Particle Physics addresses studies of the structure of the smallest components the world is made of. The Standard Model of Particle Physics (SM), which evolved from theoretical ideas and is supported by experimental facts, can successfully describe many phenomena. Still many questions are open. With the Large Hadron Collider (LHC) at CERN some of these questions will be answered. For example one tries to find the postulated Higgs particle, which would explain the mass of the gauge bosons of the weak force and that of all other particles. Also one expects to find new physics beyond the SM, like supersymmetric particles, which are part of some Grand Unified Theories and which are also candidates for Dark Matter.

The most recently discovered particle of the SM is the top quark, which is the heaviest particle known today. Its mass gives constraints on the mass of the Higgs boson and because of its high weight also super-symmetric particles are expected to be found in its decay products (if super-symmetric particles exist). Therefore the knowledge of the top properties can be used to falsify the SM and other theories beyond the SM. As the top quark decays before it hadronizes one has to reconstruct its properties using its decay products. Proton-proton collisions at the LHC produce top-antitop pairs, the decay products of which can be detected and analysed. In a hadron collision top-antitop decays do not occur isolated, but many other processes are detected at the same time. These background processes have to be discriminated from the top-antitop decay. In this thesis the discrimination of the so-called W +jets background contribution is studied and how this background events behave, if interpreted as top-antitop pairs in the reconstruction of top-antitop events.

In Chapter 2, the SM is summarized with emphasis on the top quark, its production and decay. In Chapter 3 the ATLAS detector is introduced and important detector/collider relevant terms will be explained. In Chapter 4, the reconstruction of top-antitop pairs with the method of kinematic fitting, based on the Maximum Likelihood method is presented. Chapter 5 addresses the performance of the used

1. Introduction

fitting program (KLFitter) when either an electron or a muon is in the final state of semileptonic top decay. The main part of this thesis lies in Chapter 6, where the impact of the KLFitter on background with respect to signal is studied. Chapter 7 deals with the comparison of two sets of transfer functions which are used in the fitting procedure of the KLFitter. Conclusions and an outlook can be found in Chapter 8. All units in this thesis are in natural units: $\hbar = c = 1$.

2. The Top Quark in the Standard Model

The Standard Model of Particle Physics (SM) describes the fundamental forces between elementary particles and the structure of matter. In the SM matter is built up from elementary spin- $\frac{1}{2}$ particles (*fermions*). The building blocks are six *quarks* and six *leptons*, which are subject to the three fundamental forces *strong interaction*, *weak interaction* and *electromagnetic interaction*. Gravity is not included in the SM, but this fact presents no loss in predictivity of the model, as the strength of gravity on subatomic scales is negligible. Each force is mediated by spin-1 particles (*bosons*). In addition, there is a mirror particle for every type of quark and lepton with the same mass and opposite (electric) charge, the so-called antiparticles.

2.1. Particle Interactions

All quarks and charged leptons are subject to the electromagnetic force, mediated by the electrically neutral photon (γ). Only electrically charged particles participate in electromagnetic interactions. This part of the SM is mathematically formulated as a relativistic quantum field theory called *Quantum Electrodynamics* (QED). Quantum field theories (QFT) can be defined by their *Lagrangian* \mathcal{L} which is locally invariant under some unitary group (called *gauge group*). The postulation of local invariance under the gauge transformations of \mathcal{L} leads to new fields, which are interpreted as the bosons mediating the force which the QFT describes. In this terminology QED is an *Abelian gauge theory* with symmetry group $U(1)$.

Only particles carrying *colour charge* participate in strong interactions. The only fermions with colour charge are quarks. There are three different types of colour charge for quarks (*red* (r), *green* (g) and *blue* (b)) and three types of anti-colour for anti-quarks (*anti-red* (\bar{r}), *anti-green* (\bar{g}) and *anti-blue* (\bar{b})). In contrast to the

2. The Top Quark in the Standard Model

fermions	family			electric charge	colour	weak isospin		spin
	1	2	3			left handed	right handed	
leptons	ν_e	ν_μ	ν_τ	0	-	1/2	-	1/2
	e	μ	τ	-1			0	
quarks	u	c	t	+2/3	r, b, g	1/2	0	1/2
	d	s	b	-1/3			0	

Table 2.1.: Family structure of the fermions.

photon, which mediates between electrically charged particles but carries no electric charge by itself, the gluon carries the charge it mediates. Therefore gluons can interact with gluons, but photons not with photons. This theory is called *Quantum chromodynamics* and is a $SU(3)$ gauge theory with eight gluons.

One important aspect is that every observable particle built out of quarks (*hadrons*) is neutral with respect to colour charge. This means that it is impossible to observe free quarks. Quarks can be found only as pairs of quark and anti-quark which results in a colour neutral *meson* ($q\bar{q}$) or as triple of quarks or anti-quarks (*baryons*) which results also in colour neutral particles ((qqq) or $(\bar{q}\bar{q}\bar{q})$). This empirical fact is called *confinement* [1, p. 41 ff.]. In contrast to the electromagnetic force, the strength of which decreases with increasing distance of two electrically charged particles, the strength of the strong force increases with increasing distance of two quarks. Trying to divide two quarks, bound together as a meson, by pulling them apart, increases the energy of the colour field between these two quarks. At some stage it is more energy favorable to convert the energy stored in the colour field to two new quarks, which each form a new meson with the quarks which were initially pulled apart. This effect is called *hadronization* [2, p. 251-252]. All quarks and leptons are subject to the weak interaction. The weak interaction is mediated by three bosons, the W^+ (positive electric charge), W^- (negative electric charge) and Z^0 (electrically neutral).

Each of the six quarks has its own flavour quantum number called up (u), down (d), charm (c), strange (s), top (t) and bottom (b), which are conserved under strong and electromagnetic interaction, but not in weak interactions. Quarks with electric charge of $+2/3$ are called up-type, with charge $-1/3$ down-type. One can arrange the quarks and leptons in three families ordered by increasing mass. In table 2.1 the three lepton and quark families are listed [3, p. 169]. Absorbing or emitting W -bosons changes left-handed leptons and quarks (right-handed anti-leptons and

anti-quarks) from up-type to down-type or vice versa.

Up-type and down-type particles of every family are isospin partners, with isospin $T = 1/2$. This isospin formalism is called *weak isospin*. Right-handed fermions do not couple to W -bosons. Thus they have no weak isospin partner they can change into, their weak isospin T is 0. Hence, every family forms two weak isospin doublets (left-handed leptons and left-handed quarks) and three weak isospin singlets [3, p. 161]. This fact, that only left-handed particles couple to W^\pm is also formulated in the $V - A$ (vector minus axial vector) structure of the weak current, which projects out only the left-handed part of any spinor. As neutrinos have mass of zero in the SM¹ they have a velocity equal to the speed of light. Therefore their handedness cannot change under any Lorentz transformation. The only way we observe neutrinos, is under weak interactions. This means only left-handed neutrinos (right-handed anti-neutrinos) can be observed [5, p. 115] and therefore no right-handed neutrino singlets is known to exist. This formulation of weak interaction that only left-handed particles take part incorporates the empirical fact of maximal violation of parity, meaning the weak interaction is not invariant under parity transformation P with $P\psi(t, \vec{x}) \rightarrow \psi(t, -\vec{x})$. This transformation would change left-handed into right-handed particles.

If the energy of processes is high enough, the electromagnetic and weak interactions unify to the *electroweak interactions*. In the Glashow-Weinberg-Salam (GWS) model four massless, mediating bosons (W^1, W^2, W^3 and B^0) are obtained with the gauge group $SU(2) \times U(1)$. These four bosons mix to the physical bosons

$$\begin{aligned} |\gamma\rangle &= |B^0\rangle \cos \theta_w + |W^3\rangle \sin \theta_w, \\ |Z^0\rangle &= -|B^0\rangle \sin \theta_w + |W^3\rangle \cos \theta_w, \\ |W^\pm\rangle &= \frac{1}{\sqrt{2}} (|W^1\rangle \mp i |W^2\rangle). \end{aligned}$$

The angle θ_w is called *weak mixing angle* or *Weinberg angle* and is a free parameter in the GWS model. Via the *Higgs mechanism* Z^0 and W^\pm gain their masses with the appearance of a new, yet unobserved, massive particle, the *Higgs boson*. The Higgs mechanism is based on the concept of *spontaneous symmetry breaking*. This means the Lagrangian of the GWS-model \mathcal{L} is invariant under $SU(2) \times U(1)$. Selecting one specific vacuum state and formulating \mathcal{L} in terms of fluctuations around this

¹In fact, current experiments show that there is evidence of neutrinos oscillating from one flavour to another, which is only possible if the neutrino masses are greater than zero [4, p. 157].

2. The Top Quark in the Standard Model

specific vacuum state, breaks the former $SU(2) \times U(1)$ -symmetry.

2.2. CKM Matrix

The weak isospin partners of u , c and t are not d , s and b , which are the physical eigenstates (i. e. mass eigenstates) of the quarks, but d' , s' and b' which are the weak eigenstates of the three down-type quarks.

Cabibbo developed 1963 [6] the idea, that the weak eigenstates are linear combinations of the mass eigenstates for the quarks u , d and s (the only known quarks at this time). The *Cabibbo-Kobayashi-Maskawa-Matrix* (CKM-Matrix) is the extension of the Cabibbo matrix to three quark generations and indicates in which strengths the physical states mix to make up the weak eigenstates. The absolute squared entries $|V_{ij}|^2$ are the transition probabilities of quark i to (anti)-quark j .

$$\begin{pmatrix} d' \\ s' \\ b' \end{pmatrix}_L = \begin{pmatrix} V_{ud} & V_{us} & V_{ub} \\ V_{cd} & V_{cs} & V_{cb} \\ V_{td} & V_{ts} & V_{tb} \end{pmatrix} \begin{pmatrix} d \\ s \\ b \end{pmatrix}_L$$

The CKM-Matrix is unitary, meaning $\sum_{k=1}^N V_{ik}V_{jk}^* = \delta_{ij}$, with $N = 3$ the dimension of the matrix. The complex CKM matrix has $2N^2 = 18$ free parameters which reduce to $N^2 = 9$ parameters due to the $N^2 = 9$ unitary constraints. Six quark fields can absorb five relative phases, this results in four free parameters of the CKM-Matrix. One of the four parameters is a complex phase, which leads to CP -violation [7, p. 224].

One can obtain the entries of the CKM-Matrix by measuring the branching ratios of weak decaying hadrons [2, p. 426], except V_{tb} which can be calculated under the assumption that the CKM-Matrix is unitary². The measured transition probabilities are [4, p. 174]

$$\begin{pmatrix} |V_{ud}| & |V_{us}| & |V_{ub}| \\ |V_{cd}| & |V_{cs}| & |V_{cb}| \\ |V_{td}| & |V_{ts}| & |V_{tb}| \end{pmatrix} = \begin{pmatrix} 0.97419 \pm 0.00022 & 0.2257 \pm 0.0010 & 0.00359 \pm 0.00016 \\ 0.2256 \pm 0.0010 & 0.97334 \pm 0.00023 & 0.0415 \pm 0.0011 \\ 0.00874 \pm 0.00037 & 0.0407 \pm 0.0010 & 0.999133 \pm 0.000044 \end{pmatrix}.$$

²A direct measurement of V_{tb} is possible in *single top decay* discussed later on

2.3. Top Quark

The top quark is the heaviest known elementary particle and thus discovered not until 1995 as the last of the six quarks [8, 9]. With a mass of $m_t = 173.1 \pm 1.3$ GeV [10] it is almost as heavy as a gold atom. As mentioned above, it is the weak isospin partner of the bottom quark, meaning $T_3 = +1/2$, $Q = +2/3$ (electric charge). Because of its high mass, the top quark has an extremely short mean lifetime of $\tau \approx 0.5 \cdot 10^{-24}$ s. Thus the top quark decays before it hadronizes [11, p. 14].

2.3.1. Top Quark Pair Production

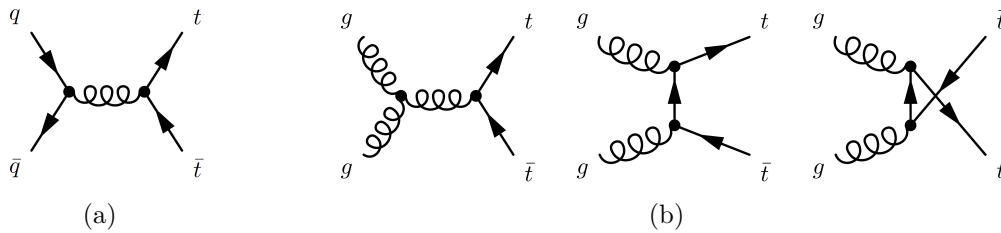


Figure 2.1.: Feynman graphs of leading order processes of $t\bar{t}$ -pair production via quark-antiquark annihilation (a) and gluon fusion (b).

Top pairs ($t\bar{t}$) are produced in proton-proton (pp) collisions at the LHC or proton-antiproton ($p\bar{p}$) collisions at the Tevatron. Pairs of top-antitop are either produced via quark-antiquark annihilation $q\bar{q} \rightarrow t\bar{t}$ or gluon fusion $gg \rightarrow t\bar{t}$. Which of these processes contributes most to the production rate depends especially on the center of mass energy, \sqrt{s} , of the collider. The square of the available energy of the partonic process ($i + j \rightarrow t\bar{t}$) is $\hat{s} = x_i x_j s$, with x_i the relative momentum fraction of the parton i . In order to produce at least a $t\bar{t}$ -pair at rest, \hat{s} has to be larger than $4m_t^2$:

$$\hat{s} > m_{t\bar{t}} = (p_t + p_{\bar{t}})^2 = m_t^2 + m_{\bar{t}}^2 + 2p_t p_{\bar{t}} > 4m_t^2.$$

Setting $x_i \approx x_j = x$ results in $x \approx 2m_t/\sqrt{s}$ for the Tevatron (Run II, $\sqrt{s} = 1.96$ TeV) and LHC of

$$\begin{aligned} x &= 0.18 \text{ (Tevatron Run II),} \\ &= 0.05 \text{ (LHC, } \sqrt{s} = 7 \text{ TeV),} \\ &= 0.025 \text{ (LHC, } \sqrt{s} = 14 \text{ TeV).} \end{aligned}$$

2. The Top Quark in the Standard Model

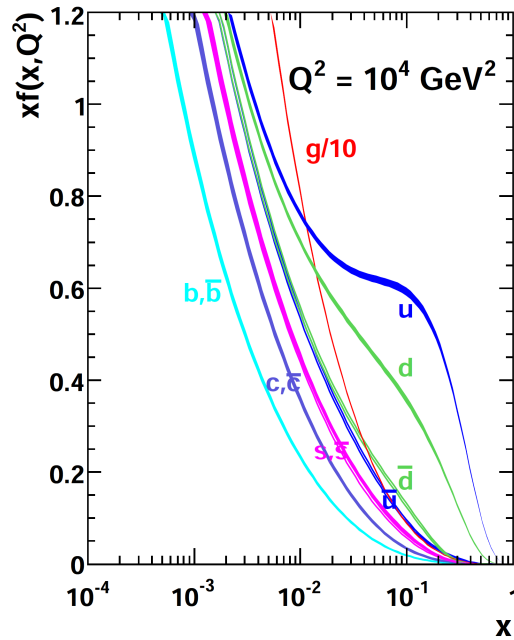


Figure 2.2.: The parton distribution function for a proton with momentum transfer of $Q^2 = (100 \text{ GeV})^2$.

As the *parton distribution function* (PDF) for small x is much higher for gluons than the PDF of valence quarks and even sea quarks (Figure 2.2), the $t\bar{t}$ -pair production at the LHC is dominated by gluon fusion [11, p. 10-12].

2.3.2. Single Top Production

As the top-pair production is via strong interaction, single top quarks can be produced in weak interactions. All these processes contain the Wtb vertex and so their cross sections are proportional to $|V_{tb}|^2$, which gives access to direct measurement of this CKM-matrix element. At the LHC the process $bg \rightarrow b \rightarrow Wt$ is expected, whereas the t -channel and s -channel processes $qq' \rightarrow W \rightarrow bt$ are also expected to be observed at the Tevatron.

2.3.3. Top Decay Topology of Top Quark Pairs

As the CKM-Matrix entry $|V_{tb}| \approx 1$, the top quark decays nearly to 100% to a b -quark and a W -boson. Thus, $t\bar{t}$ -pairs decay to

$$t + \bar{t} \rightarrow bW^+ + \bar{b}W^-. \quad (2.1)$$

As the W -bosons are also unstable, they decay. The possible decay channels are

- a) $t + \bar{t} \rightarrow bW^+ + \bar{b}W^- \rightarrow bq_1\bar{q}_2 + \bar{b}q_3\bar{q}_4,$
 $t + \bar{t} \rightarrow bW^+ + \bar{b}W^- \rightarrow bq_1\bar{q}_2 + \bar{b}\ell\bar{\nu}_\ell,$
- b) $t + \bar{t} \rightarrow bW^+ + \bar{b}W^- \rightarrow b\bar{\ell}\nu_\ell + \bar{b}q_1\bar{q}_2,$
- c) $t + \bar{t} \rightarrow bW^+ + \bar{b}W^- \rightarrow b\bar{\ell}_1\nu_{\ell_1} + \bar{b}\ell_2\bar{\nu}_{\ell_2}.$

Here q_i stands for any quark, except the top quark as this exceeds the mass of the W -boson. Because of conservation of charge q_1 and \bar{q}_2 have to be either up- and down- or down- and up-type. ℓ_i indicates a lepton of any kind and ν_{ℓ_i} the appropriate neutrino. The decay mode a) is called *hadronic channel* as the final state of the $t\bar{t}$ -decay consists of quarks only, which hadronize before they are detected. Decay mode b) is called *semileptonic channel* because half of the W -bosons decay

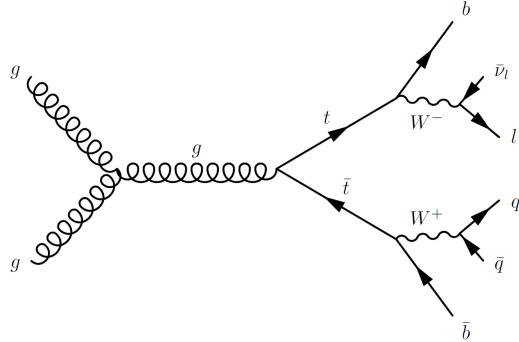


Figure 2.3.: Feynman graph of $t\bar{t}$ -pair produced via gluon fusion and decaying semileptonically.

into leptons. The last mode c) is called *dileptonic channel* (see Figure 2.3).

From the CKM-Matrix again, it can be seen, that the hadronically decaying W decays mostly into a quark and an antiquark of the same generation. The possible

2. The Top Quark in the Standard Model

Decay mode	branching on born level	QCD fractions [12, p. 17]
hadronically	4/9	45.5%
semileptonically	4/9	43.5%
leptonically	1/9	10.5%

Table 2.2.: Branching ratios in $t\bar{t}$ -decay. The simple considerations mentioned here, show good agreement with the QCD calculations of leading order (QCD fractions).

final states of the hadronically decaying W are therefore $u\bar{d}$ or $s\bar{c}$, with both coming in three different colour neutral states $r\bar{r}$, $g\bar{g}$ and $b\bar{b}$. This results in 36 different decays of the hadronic $t\bar{t}$ -decay.

As the W mass is much larger than the masses of the quarks and leptons it decays into, *fermion universality of the weak interaction* holds. Thus one concludes that the probability of the W -boson decaying into quarks ($q_1\bar{q}_2$) or leptons ($\ell\bar{\nu}$) is approximately the same and also the same for the different families. There are three different states the W^- boson can decay into leptonically: $e^-\bar{\nu}_e$, $\mu^-\bar{\nu}_\mu$ and $\tau^-\bar{\nu}_\tau$ (analogously for the W^+ boson). This results in 36 different final states the $t\bar{t}$ -pair can decay into semileptonically, because every state can be reached via two paths (either the W^+ or the W^- boson decays hadronically).

For the full leptonic decay (dileptonic channel), just nine different paths are possible.

This results in a total number of 81 possible decay paths. In Table 2.2 the branching ratios are listed. The semileptonic channel (or *lepton+jets* channel) features a high branching ratio and manageable background, as the signature of four high energetic jets and one high energetic charged lepton with additionally missing energy from the undetectable neutrino can be well distinguished from background processes. The hadronic channel (or *all jets* channel) features the highest branching ratio but has the drawback of huge multijet background. The leptonic channel features the lowest background, as the number of possible background processes with two high energetic, charged leptons and jets is small. But this channel has the lowest branching ratio.

2.3.4. Tau Leptons in the Final State

As the τ lepton has a short lifetime of approximately $3 \cdot 10^{-13}$ s [4], it decays before it covers the distance from the center of the beam pipe to the detector. The dominant decay paths are

$$\begin{aligned}\tau^- &\rightarrow \mu^- \bar{\nu}_\mu \nu_\tau \text{ (17\%),} \\ \tau^- &\rightarrow e^- \bar{\nu}_e \nu_\tau \text{ (18\%),} \\ \tau^- &\rightarrow \nu_\tau + \text{hadrons (62\%).}\end{aligned}$$

Thus, one counts a $t\bar{t}$ -decay only as semileptonic or leptonic if the leptons in the final state are e or μ . With this restriction the branching ratios change to 45.5%, 29% and 4.7% (same order as in Table 2.2) [12].

2.4. Background Processes to Top-Antitop Decay

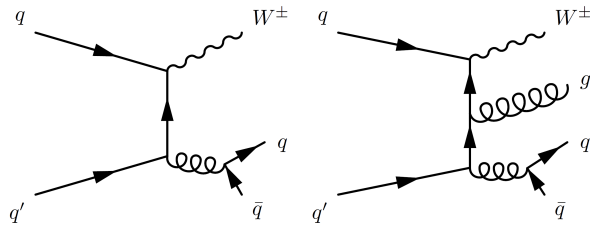


Figure 2.4.: Two exemplary Feynman graphs of W +jets background processes (W + 2 partons, W + 3 partons).

The main *physical* background sources in the semileptonic channel at a hadron collider are

- $W + \text{jets} \rightarrow \ell \bar{\nu}_\ell + \text{jets}$ (wjets)
- $t \rightarrow W b \ell \rightarrow \ell \bar{\nu}_\ell + \text{jets}$ (single top)
- $WZ \rightarrow \ell \bar{\nu}_\ell + \text{jets}$
- $Z^0 + \text{jets}$

The W +jets background is most relevant for the semileptonic channel, since the lepton in this background process comes from W -decay, just like in the leptonic top

2. The Top Quark in the Standard Model

decay. The jets come from higher order processes (Initial State Radiation (ISR), Final State Radiation (FSR)) or other interacting partons³. Two exemplary Feynman graphs of this process are shown in Figure 2.4. The WZ and single top background is less important as the cross section is lower than from $t\bar{t}$. Z^0 +jets background is only relevant for the dileptonic channel but not for semileptonic channel because the Z^0 does not decay into neutrinos (disregarding $Z^0 \rightarrow \tau\bar{\tau}$, with the τ 's decaying leptonically).

In addition *instrumental* background exists. These are QCD multijet events with “fake” leptons, this means jets are detected as electron (“fake electrons”) or real muons are detected as isolated muons, because the b -jet of the corresponding semileptonically b -decay is not reconstructed (“fakly isolated muons”).

³Interacting partons, which do not make up the W , but belong to the same hadron-hadron collision, are meant here.

3. Atlas Detector

The ATLAS (**A** toroidal **LHC** apparatus) detector is one of four experiments at the LHC (*Large Hadron Collider*) at the CERN site. The overall layout of the 25 m high, 44 long and approximately 7000 t heavy detector is shown in Figure 3.1. In the inner

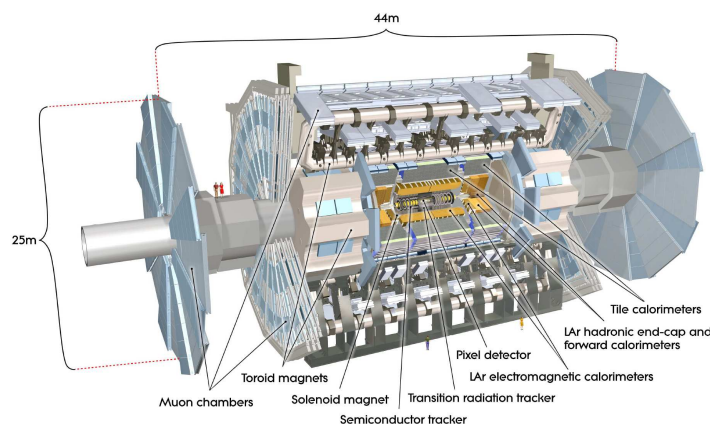


Figure 3.1.: The overall layout of the ATLAS detector.

detector momentum and vertex measurements, as well as electron identification are achieved. The inner detector is immersed in a 2 T solenoidal magnetic field and consists of semiconductor pixel, strip detectors and a Transition Radiation Tracker (TRT). The electromagnetic calorimeters are liquid Argon (LAr) sampling calorimeters, whereas the hadronic calorimeter is provided by a scintillator-tile calorimeter (except the end-cap calorimeters, which are also build on LAr technology). The calorimeter is covered by the muon chambers, which define the overall size of ATLAS.

The interaction rate of the LHC is designed for approximately 1 GHz, while the event data recording is limited to about 200 Hz. This requires trigger systems to decide whether an event should be rejected or not. The Level-1 (L1) trigger reduces the data rate to about 75 kHz. The Level-2 trigger and event filter provide the reduction to the data taking rate of 200 Hz. The general performance goals of the

3. Atlas Detector

ATLAS detector [13] are for the electromagnetic calorimeter

$$\frac{\sigma_E}{E} = \frac{10\%}{\sqrt{E}} \oplus 0.7\%.$$

The energy resolution of the hadronic calorimeter is supposed to reach

$$\frac{\sigma_E}{E} = \frac{100\%}{\sqrt{E}} \oplus 10\%.$$

The required transverse momentum resolution for the muon spectrometer is

$$\frac{\sigma_{p_T}}{p_T} = 10\% p_T.$$

All energies and momenta are in units of GeV¹, the index T stands for “transverse” ($p_T = \sqrt{p_x^2 + p_y^2}$). In particle physics the direction of particles is measured in ϕ and pseudorapidity η , instead of the angles of spherical coordinates ϕ and θ . Pseudorapidity is defined as $\eta = -\tan \frac{\theta}{2}$. The reason for using η is that in the high energy approximation the differential cross section $\frac{d\sigma}{d\eta}$ is Lorentz invariant. Using the definition of η it can be seen that the direction parallel to the beam is $\eta = \pm\infty$, whereas orthogonal to the beam means $\eta = 0$. All three mentioned detector parts cover an η -range of ± 2.5 , with the forward hadronic calorimeter expanding the η -range up to $|\eta| < 4.9$. From now on the z -axis is the axis parallel to the direction of the beam pipe and the point of origin of the coordinate system lies in the interaction point of the ATLAS detector.

In a proton-proton collision at the LHC the total momentum of the colliding protons is balanced (zero), but not the total momentum of the initial partons which annihilate or fuse to a $t\bar{t}$ -pair. Thus the total momentum of all detected particles in one event is generally not zero. But in the plane orthogonal to the beam direction the total momentum of all detected particles of an event is close to zero, as the colliding protons have only small momentum in this plane.

The neutrino cannot be detected and therefore adding up the transverse momenta of all detected particles of one event does not add up to zero, if there was a neutrino. The missing transverse momentum² is often written as \cancel{E}_T and indicates undetected particles.

¹Appropriate powers of GeV have to be inserted into the above formulas, to end with σ_E/E without units.

²The terms *missing transverse energy* and *missing transverse momentum* are the same

4. Kinematic Fitting

A particle has a *true* momentum and energy value (disregarding Heisenberg's uncertainty principle). As the detector is not an ideal measuring instrument, it measures momenta and energies with a certain resolution. This means the measured values are distributed around the true values. This distribution can be determined and parametrized into functions, called *transfer functions*.

If one measures an event and knows the topology of this event one can use the information about momentum and energy conservation at the decay vertices to vary the measured values in that way, that they fit the considered event topology best. This procedure is called *kinematic fitting* [14, p. 141] and can be done with a *likelihood Ansatz*. With this method, also unmeasured quantities can be reconstructed from the measured data¹.

4.1. Maximum Likelihood Method

The *Maximum Likelihood Method* (ML) is a method to construct an estimator \hat{a} for a quantity a . The parameter a describes the probability of measuring a certain data sample $\{x_1, \dots, x_N\}$ drawn from a probability density function $p(x; a)$. The probability for measuring the data set $\{x_1, \dots, x_N\}$ as a function of the parameter a is called *Likelihood function* L and can be obtained by the individual probabilities of every single data point:

$$L(x_1, x_2, \dots, x_N; a) = p(x_1; a)p(x_2; a) \dots p(x_N; a) = \prod_{i=1}^N p(x_i; a).$$

The estimator \hat{a} of the parameter a under the condition of the given data set $\{x_1, \dots, x_N\}$ is that value of a , which maximizes the Likelihood function [15, p. 71-73, 81-89]. For technical reasons, one does not maximize L , but minimizes $-\log L$. Maximizing the logarithm is equivalent to maximizing the likelihood function it-

¹if the information about the event topology supplies enough constraints.

4. Kinematic Fitting

self as the logarithm is strictly monotonic. To minimize $-\log L$ one has to solve (numerically)

$$-\left. \frac{\partial \log L}{\partial a} \right|_{a=\hat{a}} = \sum_{i=1}^N \left. \frac{\partial \log p(x_i; a)}{\partial a} \right|_{a=\hat{a}} = 0.$$

ML estimators are usually *consistent* ($\lim_{N \rightarrow \infty} \hat{a} = a$) but *biased*. In the asymptotic limit ($N \rightarrow \infty$) the ML estimator is unbiased (like any consistent estimator) and *efficient*² [15, p. 85]. The method of χ^2 -fitting can be derived as a special case from the ML method if one uses Gaussian distributions for the individual probability distributions $p(x_i; a)$. In most cases the *Central Limit Theorem* takes care, that the measured data is Gaussian distributed around the true data. But if the $p(x_i; a)$ are not Gaussian and known, one uses the more general ML principle.

4.2. The Kinematic Likelihood Fitter (KLFitter)

The program used in this bachelor thesis is called **Kinematic Likelihood Fitter** [16] (KLFitter). This program is written in C++ and uses the ROOT Analysis Framework [17] and the **Bayesian Analysis Toolkit** (BAT) [18]. With this program it is possible to fit measured data or Monte Carlo generated and detector simulated $t\bar{t}$ -events and reconstruct quantities of the $t\bar{t}$ -decay, which cannot be measured directly, like the W mass or top mass, etc.

The nomenclature of the particles in the final state of the semileptonic $t\bar{t}$ -decay is as follows. The final state consists of four quarks, which are measured in the detector as jets. The jet associated with the b -quark coming from the top decaying hadronically (leptonically) is called hadronic (leptonic) b -jet. One W -boson decays into two quarks which are called *light quarks*. If the detected jets originating from these quarks are meant, they are called *light jets*.

The KLFitter uses the following measured values to fit the $t\bar{t}$ event:

- the energies and directions of the four jets associated with the four jets coming from the $t\bar{t}$ event, $\tilde{E}_i, \tilde{\Omega}_i = (\tilde{\eta}_i, \tilde{\phi}_i)$ (12 values),
- the energy and direction of the charged lepton $\tilde{E}_{\text{lep}}, \tilde{\Omega}_{\text{lep}}$ (3 values).
- the missing energy \cancel{E}_T in the transverse plane (2 values).

² $V(\hat{a}) = -\left\langle \frac{d^2 \log L}{da^2} \right\rangle^{-1}$, the variance of the ML estimator equals the minimum variance bound for $N \rightarrow \infty$.

4.2. The Kinematic Likelihood Fitter (KLFitter)

This adds up to a set of 17 measured quantities for every event. As the direction of the charged lepton is assumed to be precise, only 15 out of the 17 quantities are fitted. The distribution of these 15 quantities around their true value is described by the *transfer functions*: $W(\tilde{x}|x)$ is the probability density of measuring \tilde{x} under the condition of the true value x . The naming convention is as follows:

- $W(\tilde{E}_i|E_i)$ is the probability density of measuring \tilde{E}_i under the condition of the true energy E_i ,
- $W(\tilde{\Omega}_i|\Omega_i) = W(\tilde{\eta}_i|\eta_i)W(\tilde{\phi}_i|\phi_i)$ is the probability of measuring $\tilde{\Omega}_i$ under the condition of the true direction Ω_i .
- $W(\not{E}_x|p_x^\nu)W(\not{E}_y|p_y^\nu)$ is the transfer function of the x and y component of missing transverse energy with the true x and y component of the neutrino's momentum.

The constraints at the decay vertices are implemented via *Breit-Wigner-distributions* $BW(m; \Gamma, M)$ with pole M , width Γ and variable m .

- The invariant mass at the $W \rightarrow q_1 q_2'$ vertex has to be Breit-Wigner distributed around the W -pole mass of $M_W = 80.4$ GeV. Thus the invariant mass m_{jj} of the two jets originating from the W -decay should maximize $BW(m_{jj}; \Gamma_W, M_W)$.
- The invariant mass at the $W \rightarrow \ell \bar{\nu}_\ell$ vertex has also to be Breit-Wigner distributed around the W -pole mass. Thus the invariant mass $m_{\ell \bar{\nu}_\ell}$ of the charged and neutral lepton originating from the leptonic W -decay has to maximize $BW(m_{\ell \bar{\nu}_\ell}; \Gamma_W, M_W)$.
- The invariant mass at both $t \rightarrow Wb$ vertices has to be Breit-Wigner distributed around the top pole mass (M_t). Thus the invariant mass m_{jjj} of the three jets originating from the hadronically decaying top has to maximize $BW(m_{jjj}; \Gamma_W, M_t)$ and the invariant mass $m_{j \ell \bar{\nu}_\ell}$ of the jet and the leptons originating from the leptonically decaying top has to maximize $BW(m_{j \ell \bar{\nu}_\ell}; \Gamma_t, M_t)$.

For the calculation of the invariant mass $m_{\ell \bar{\nu}_\ell}$ the z -component of the neutrino momentum is needed and used as a free parameter in the fit. Also the mass of the top, M_t , can be treated as an optional free parameter, leading to 16 or 17 free

4. Kinematic Fitting

parameters to fit, respectively.

Hence, the Likelihood function is given by

$$L = \left(\prod_{i=1}^4 W(\tilde{E}_i | E_i) \right) \cdot W(\tilde{E}_\ell | E_\ell) \cdot W(\cancel{E}_x | p_x^\nu) \cdot W(\cancel{E}_y | p_y^\nu) \cdot \left(\prod_{i=1}^4 W(\tilde{\Omega}_i | \Omega_i) \right) \cdot BW(m_{jj}; \Gamma_W M_W) \cdot BW(m_{\ell\bar{\nu}_\ell}; \Gamma_W, M_W) \cdot BW(m_{jjj}; \Gamma_t, M_t) \cdot BW(m_{j\ell\bar{\nu}_\ell}; \Gamma_t, M_t).$$

4.2.1. Jet-to-Quark Mapping

Because of the flavour, charge and mass blindness of jets (without b -tagging) it is not known which jet originates from which quark.

One issue is, that the detector can detect more or less than four jets coming from four quarks or gluons for different reasons (ISR, final FSR, choice of jet algorithm, undetected jets, etc.). This cannot be solved with a data analysis program. As *best guess* one selects the four jets with most transverse energy. This selection rule is of course defective as it is possible that jets are selected which do not originate from the final state quarks, or one quark leads to more than one detected jets.

There are $4! = 24$ different possibilities to map the 4 measured jets to the 4 true quarks. As the likelihood function is invariant under interchanging the two light quarks, there are only 12 possible jet-to-quark mappings.

Thus the fitting procedure has to be done for all 12 combinations. The combination with the highest $\log L$ is the most likely jet-to-quark mapping and is called *best combination*. But it is possible that this combination is not the true jet-to-quark mapping. This can have two different reasons. First: none of the 12 combinations is the true combination, because the four selected jets do not belong uniquely to the four quarks (ISR, FSR, etc.). Second: One of the 12 combinations is the true combination, but the KL Fitter labels not this combination as *best combination*. For events, belonging to the latter class, it is possible to perform *truth matching*³.

4.2.2. Event Selection

As mentioned before, the topology of such events consists of one charged lepton (electron or muon), four quarks (resulting in an ideal case in four jets) and one neutrino (resulting in missing transverse energy). The selection rules are the following and their reason will be explained afterwards.

³This will be explained in the beginning of Chapter 5, later on.

- Select all leptons and jets with $|\eta| < 2.5$.
- Require a minimum of 4 jets with $p_T > 20$ GeV.
- Require a minimum of 3 jets of the latter 4 jets having $p_T > 40$ GeV.
- Require exactly one electron or muon with $p_T > 20$ GeV.
- Require $\cancel{E}_T > 20$ GeV.
- If one of the last four steps is not fulfilled, reject the whole event.

Detectors measure best in the central region and there is no detector in the beam pipe, particles with high η are detected badly. The η -range of the tracker device⁴ in the ATLAS detector is $|\eta| < 2.5$, which explains the selection on $|\eta|$. Because the top quark is heavy, one expects the decay products to be of very high energy. This means that the decay products have high transverse momentum, p_T , and the event has high missing transverse energy, \cancel{E}_T , this then enters the selection criteria.

4.2.3. In- and Output of the KLFitter

The KLFitter uses as input a sample containing the four-vectors of all jets and charged leptons of every event, as well as the missing transverse energy in the plane orthogonal to the beam pipe. For every selected event the log-likelihood, $\log L$, will be maximized by varying the four-vectors of the selected jets and leptons for all 12 combinations. The fitted four-vectors of the four jets and the charged and neutral lepton, as well as the reconstructed four-vectors of the W -bosons and the top quarks for all twelve combinations are the output of the KLFitter. The input will be referred to as *measured data*, even if it is Monte Carlo (MC) generated data. The output will be called *fitted data* and the fitted data in the combination with the highest $\log L$ is called *best*.

Producing MC generated data involves the following steps: First the *hard processes* and subsequent decays are generated with MC@NLO [19]. Secondly the partons are *showered*, this means the generation of additional partons if (for example) the distance of two quarks increases. In a third step all generated partons are *hadronized*. The last two steps are carried out by HERWIG [20]. In a last step a detector

⁴Transition radiation tracker to detect ionising particles

4. Kinematic Fitting

simulation is performed to obtain the *measured data*. MC samples can contain additionally *truth data*, which contains the four-vectors of the MC generated event (top quarks, W -bosons, b -quarks, light quarks, charged and neutral lepton), without applied parton shower, hadronization and detector simulation.

4.3. Transfer Functions

The η coverage explains the η -cut in the selection of the KLfitter, whereas the energy resolution motivates the most simple transfer functions. The muon transfer function used in the next section for fitting $t\bar{t} \rightarrow \mu + \text{jets}$ is a simple Gaussian distribution.

$$W(\tilde{p}_T|p_T)dp_T = \frac{1}{\sqrt{2\pi}\sigma_{p_T}} \exp\left(-\frac{1}{2}\left(\frac{\tilde{p}_T - p_T}{\sigma_{p_T}}\right)^2\right)dp_T. \quad (4.1)$$

As σ_{p_T} is proportional to p_T^2 ($\sigma_{p_T} = \sigma \cdot p_T^2$) one transforms the variables in the transfer function as follows: $p_T \rightarrow p_T/p_T^2 = x$ and $\tilde{p}_T \rightarrow \tilde{p}_T/p_T^2 = \tilde{x}$. This leads to

$$W(\tilde{x}|x)dx = -\frac{1}{\sqrt{2\pi}\sigma} \exp\left(-\frac{1}{2}\left(\frac{\tilde{x} - x}{\sigma}\right)^2\right)dx. \quad (4.2)$$

The minus sign or any other proportionality does not change the maximum of $\log L$, as a factor in the likelihood leads to a summand in the log likelihood. A constant summand vanishes when differentiating with respect to the free parameters.

After the transformation the width of the transfer function is independent of p_T . This makes the extraction of σ from MC generated events more easy, because only a Gaussian distribution with one free parameter σ has to be fitted to the MC generated data.

The transfer functions for the jet and electron directions are also single Gaussian distributions but for the energies they are more complicated double Gaussian functions with more than one parameter, depending on the energy. As the detector parts change over the full range of η the resolution depends on η . Thus the transfer functions are extracted for three different η -ranges. In Chapter 7 the energy resolution of jets and electron of two different sets of transfer function will be studied.

5. Fitting muon+jets Final States

In this section, the performance of the KLFitter on a sample with $t + \bar{t} \rightarrow b\bar{b}q'q + \mu\nu_\mu$ ($\mu+jets$) in comparison to the performance on a sample with $t + \bar{t} \rightarrow b\bar{b}q'q + e\nu_e$ ($e+jets$) is studied. Both samples consist of Monte Carlo generated and detector simulated events. The samples contain also *truth data*.

The first test of performance of the fitter can be done by comparing the reconstruction efficiencies (Fig. 5.1). The reconstruction efficiency is the percentage of *truth*

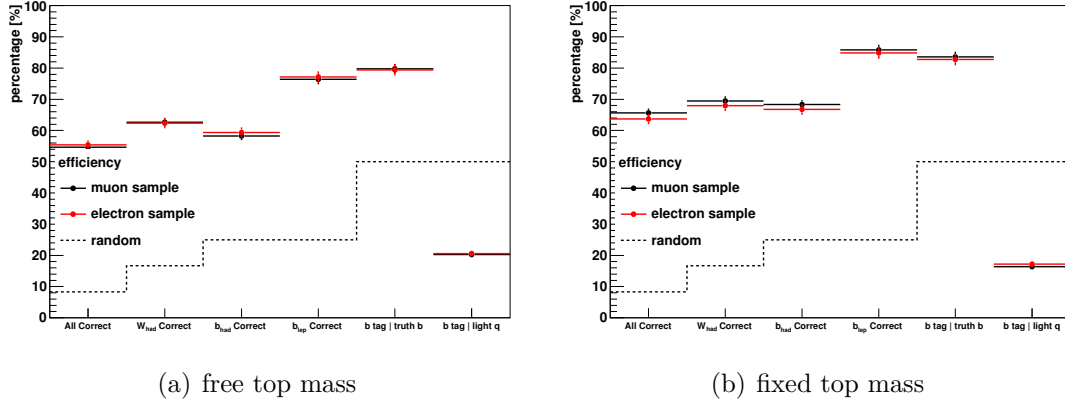


Figure 5.1.: Reconstruction efficiencies of $\mu+jets$ and $e+jets$ sample.

matched events, in which the fitter has mapped all measured jets to the truth quarks in the true combination.

Matched events are a special class of all events and make up about 20%. They contain only events in which each *truth* quark is matched with exactly one of the *measured* jets selected by the KLFitter. *Matched* means that the distances of truth quarks and measured jets are smaller than $\Delta R = \sqrt{\Delta\phi^2 + \Delta\eta^2} < 0.3$.

In Fig. 5.1 the bins from left to right have the following meaning

- *All correct* indicates the percentage of events in which all four jets were correctly assigned to truth quarks. That is the jet the KLFitter assigns to be the hadronic b -quark is truly originating from the hadronic b -quark, etc.

5. Fitting μ +jets Final States

- The second bin indicates the percentage of events, where only the decay particles of the hadronic W -boson, the light quarks, are mapped to the truth light quarks.
- The third and fourth bin show the percentage of events where at least the hadronic (leptonic) b -quark was mapped to the right jet, respectively.
- The fifth bin shows the efficiency of the KLFitter mapping any b -jet to a b -quark.
- And the last bin shows the efficiency that a b -jet is wrongly mapped to a light quark.

First of all the KLFitter has higher efficiencies in all listed cases, as randomly mapping the quarks to jets (dotted line). The efficiency plot also shows that it is easier to map the leptonic b -quark to the true jet than mapping the hadronic b -quark to the true jet. This can be explained by the fact that the $t\bar{t}$ decay can often be separated into two hemispheres, a hadronic and a leptonic hemisphere. This means that there is only one jet in a similar direction as the charged lepton. For the hadronic b -quark however there are three jets, where two have to add up to the mass of the W -boson. The efficiency of the μ +jets and e +jets sample are the same within the uncertainties. When the KLFitter is operated in the fixed top mass mode, meaning the top mass in the Breit-Wigner-distribution in the log likelihood is fixed to the true top mass which was used in the MC generator (172.5 GeV), the efficiencies rise. For example the “all correct” reconstruction efficiency of the e +jets sample rises from nearly 56% to nearly 64% (reconstruction efficiency increases by 14%). The efficiency rises by 22% for the μ +jets sample.

As the efficiencies are based only on about 20% of all fitted events, these numbers cannot be a final indicator of the performance of the KLFitter. In figure 5.2 four top mass distributions are drawn for the reconstructed top mass of the hadronic top. The *MC truth* distribution¹ shows the top mass calculated from the truth hadronic top four-vector, the *fit, best* is calculated from the invariant mass of the fitted four-vector gained by adding up the four-vectors of the two light jets and the hadronic b -jet, where the jets are assigned to quarks according to the best combination. The dotted distribution is obtained by adding up the measured four-vectors of the same jets used for the *fit, best* distribution. The only difference of these two distributions

¹Which is of course just a Breit-Wigner distribution with its peak at 172.5 GeV.

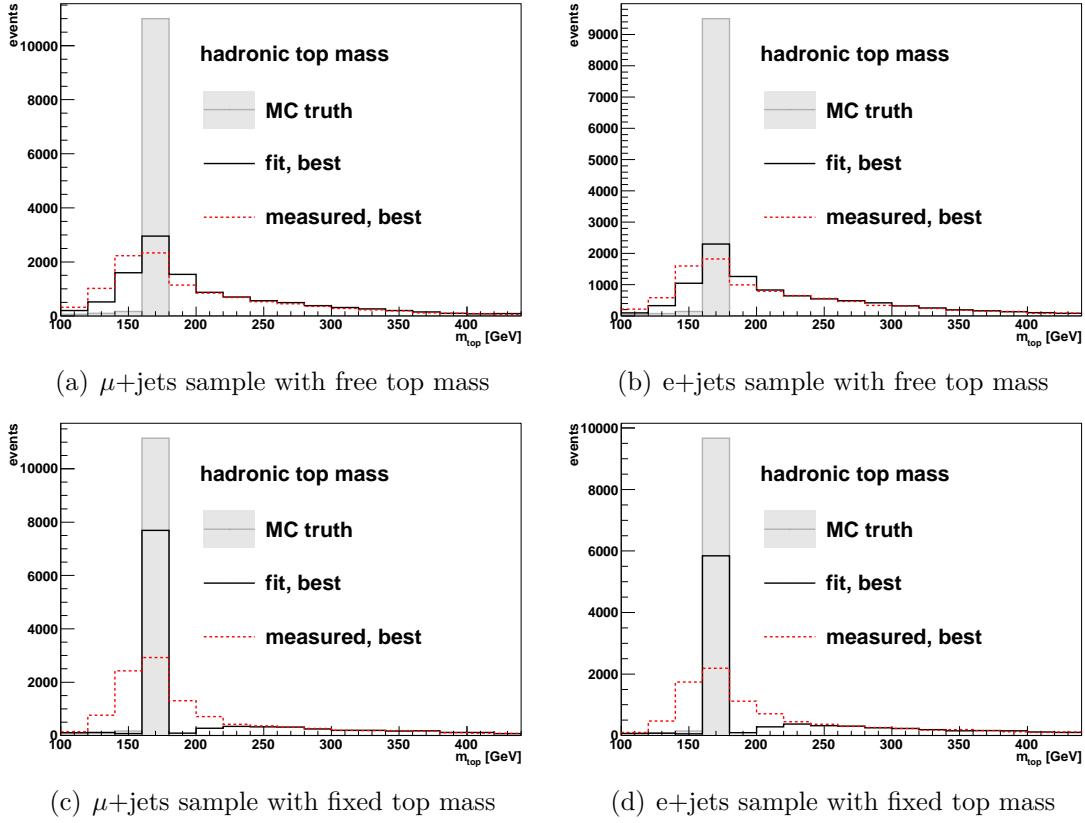


Figure 5.2.: Hadronic top mass of e+jets and μ +jets sample.

is that for the first distribution the fitted energies and momenta are used and in the second the measured values are used.

One observes that the fitted and measured distribution match the MC truth value in the fixed top mass mode better. This can be expected because there is one free parameter less to fit. If in the KLFitter the mass is fixed to the true top mass the fitted top mass distribution does not need to match the truth distribution a priori, as the top mass distribution is obtained from the invariant mass of the reconstructed top quark. In addition, the differences between measured and fitted distribution increase when fixing the top mass while fitting. This means that the fitter has a larger effect on the data.

Also, one observes that the fraction of fitted events which match the peak of the MC truth distribution is higher for the μ +jets sample compared to the e+jets sample.

Figure 5.3 shows the measured, fitted and MC truth distributions of the transverse momentum p_T of the leptonic top quark. In the same way as in the top mass plots, the fitted and measured distributions match the MC truth distribution better in

5. Fitting muon+jets Final States

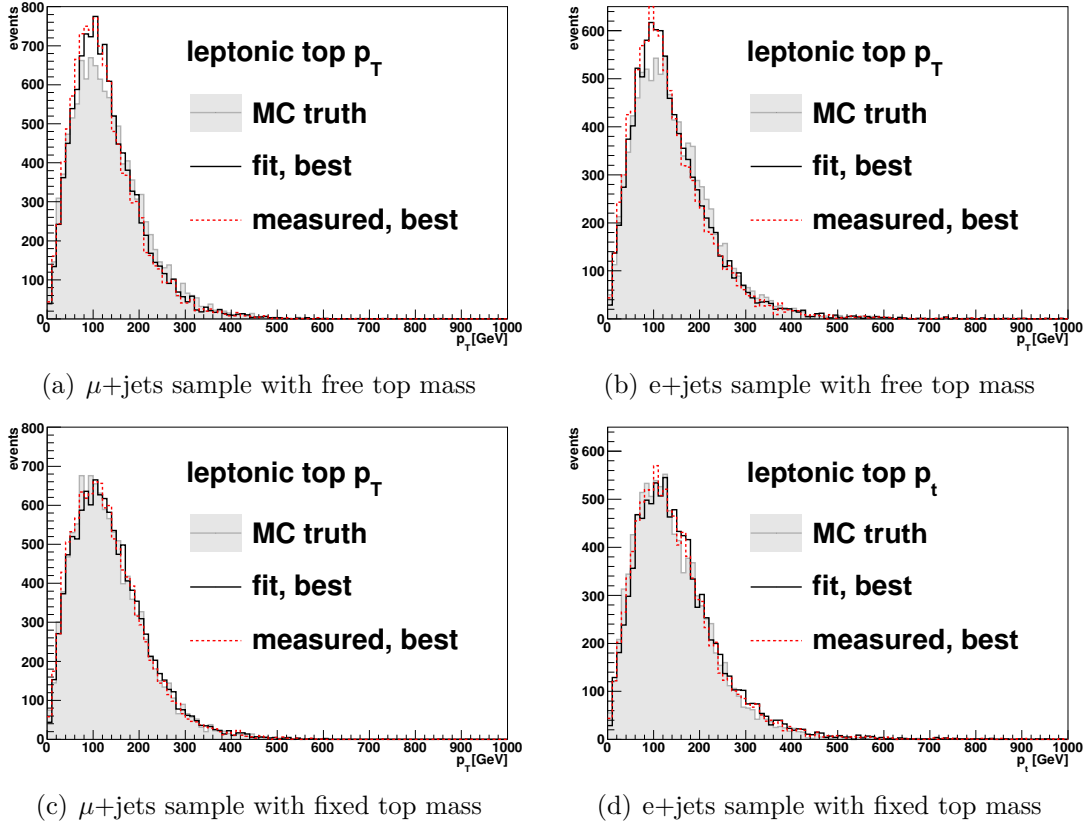
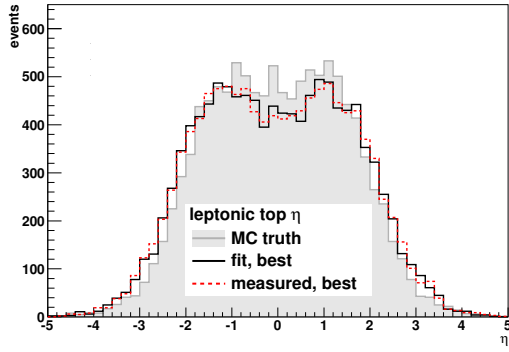


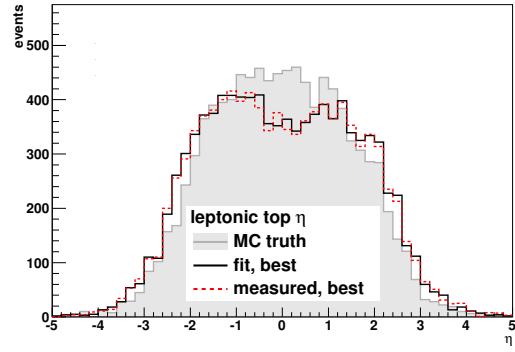
Figure 5.3.: Leptonic top p_T of e+jets and μ +jets sample.

the case of a fixed top mass. In contrast to the top mass distributions the variation between the measured and fitted distributions seem to be small. This does not mean that the KLFitter does nothing, as the best combination and the four-vector of the top quarks would not be known without the fitter. The agreement of measured with the truth distribution shows, that the fitter often finds the true jet-to-quark combination. No qualitative differences between the μ +jets and e+jets sample can be observed.

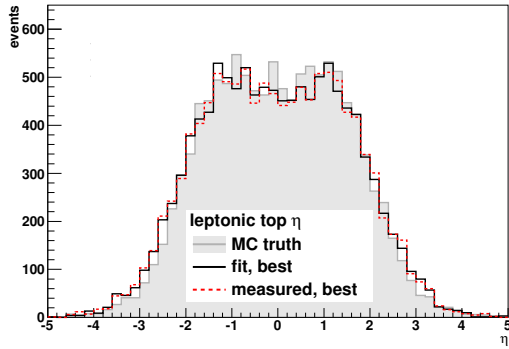
In Figure 5.4 the η distribution of the measured, fitted and MC truth data is plotted. Operating the KLFitter in fixed top mass mode shrinks the width of the fitted distribution in the way that it fits the MC truth distribution better. This effect is more obvious for the e+jets sample than for the μ +jets sample, as here the truth and fitted distribution matches even for the free top mass mode quite well. But for both samples the “dip” in the central η -region disappears when fixing the top mass. In this chapter the distributions of hadronic top mass, leptonic top p_T and η were discussed. The distributions for the leptonic top mass, hadronic top p_T and η are



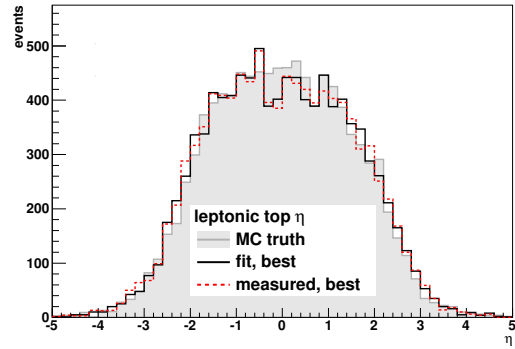
(a) μ +jets sample with free top mass



(b) e+jets sample with free top mass



(c) μ +jets sample with fixed top mass



(d) e+jets sample with fixed top mass

Figure 5.4.: Leptonic top η of e+jets and μ +jets sample.

qualitatively the same and can be found in the Appendix A.

6. Fitting Background

In the next sections, the behaviour of the KL Fitter on background is studied with respect to its performance on signal.

6.1. Used MC Samples

For background, MC samples with $pp \rightarrow W + \text{jets} \rightarrow e\bar{\nu}_e + \text{jets}$ (*wjets*) and $t\bar{t} \rightarrow e\bar{\nu}_e + \ell\bar{\nu}_\ell$ (dileptonic channel of $t\bar{t}$ decay, *dilep*) are used. The *wjets* MC sample contains events with $W + 0$ partons, $W + 1$ parton, \dots , $W + 5$ partons. Because of initial state radiation, final state radiation and detector specific effects (jet reconstruction algorithm, undetected jets, etc.) more or less jets as partons can be detected. This means that the jet multiplicity of these samples after the detector simulation can be different from the parton multiplicity.

$t\bar{t} \rightarrow e\bar{\nu}_e + \text{jets}$ events are used as signal sample (*ejets*). Both *ejets* and *dilep* sample come from the same $t\bar{t} \rightarrow \ell\bar{\nu}_\ell + X$ sample, which contains semileptonic and dileptonic $t\bar{t}$ events. By selecting events with an electron and a second lepton (electron or muon) only, the *dilep* sample was obtained. In the same way the *ejets* sample was produced by selecting only events with one electron. Thus the Table 6.1, which shows the cross sections calculated by the MC generator, does not list *ejets* or *dilep* explicitly, but the whole signal sample. All samples are generated at a center of mass energy of $\sqrt{s} = 7$ GeV.

6.2. Signal and Background without Selection

To be precise: a preselection was done with $p_T > 15$ GeV and $N_{\text{jets}} \geq 1$, but not the full selection explained in Chapter 4.2.2.

As the KL Fitter needs at least four jets, Figure 6.1 shows that the requirement of $N_{\text{jets}} \geq 4$ rejects the very most part (93%) of *wjets* background, the most part

6. Fitting Background

sample	cross section [pb]	generated events	weight
$t\bar{t} \rightarrow e + X$	87.4	999,387	0.024
wjets 0 partons	8,434.2	1,381,931	1.648
wjets 1 partons	1,577.5	258,408	1.649
wjets 2 partons	460.0	188,896	0.658
wjets 3 partons	123.1	50,477	0.659
wjets 4 partons	30.9	12,991	0.642
wjets 5 partons	8.4	3,449	0.659

Table 6.1.: Cross section from MC generator for the used samples (LO for wjets and NLO for $t\bar{t} \rightarrow e + X$, scaled by the k -factor to achieve an approximation for NLO and NNLO, respectively). The weight is used to scale the number of generated events to an integrated luminosity of $270(\text{pb})^{-1}$ (arbitrary value).

(58%) of dilep background and keeps the most (84%) of the signal (ejets). The jet multiplicity is as one expects: The ejets sample has on average a little bit more than four jets per event with four jets expected, for the dilep sample the jet multiplicity is on average lower, one expects at least two jets because of the two b -quarks. The lowest jet multiplicity on average can be observed for the wjets sample, which is also consistent, because the cross section for wjets events with low parton multiplicities are the highest. The reason for this is that the matrix element \mathcal{M} gets for every additional parton an additional factor of $\alpha_s < 1$ (strong coupling constant): $\sigma \propto |\mathcal{M}|^2 \propto \alpha_s^{n_{\text{jets}}}$.

The p_T distribution of jets in Figure 6.2(a) shows that jets in the wjets sample have on average lower energy than jets from $t\bar{t}$ -decay. This is expected as the jets in the wjets sample do not come from top decay but from QCD processes where the available energy is less than M_t . The same can be said for the p_T distribution of the electron in the three samples (Figure 6.2(b)). In the wjets sample the electron comes from a W -decay but as the W does not come from top decay the available energy for the electron is on average smaller than in the ejets sample. The dilep sample follows the p_T distribution of the ejets sample as expected. The jet p_T of the dilep sample is on average a little bit lower than of the ejets sample because in the dilep sample one expects two high energetic jets (b -quarks) and for the ejets sample four high energetic jets. The electrons in Figure 6.2(b) come from top decay for the ejets sample as well as for the dilep sample. As the distributions are normalized to one, there is no difference expected and also no difference observable.

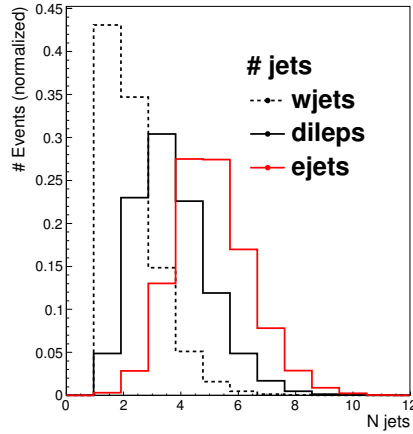


Figure 6.1.: This figure shows the jet multiplicity distribution per event for signal and background before selection.

6.3. Effect of the Event Selection

The event selection introduced in Section 4.2.2 rejects 95% of the wjets background and 89% of the dilep background, whereas only 66% of the signal (ejets) are rejected (see Table 6.2). But still the wjets background contributes most events (60%) to the total number of signal+wjets+dilep events (see Figure 6.3).

Sample	events before selection	events after selection	rejection	summarized rejection
ejets	174,371	59,899	66%	66%
dilep	76,050	8,392	89%	89%
wjets 0 partons	0	0	100%	
wjets 1 partons	139,282	4	> 99.9%	
wjets 2 partons	116,922	126	> 99.8%	95%
wjets 3 partons	32,404	677	98%	
wjets 4 partons	8,470	1,024	88%	
wjets 5 partons	2,261	645	71%	

Table 6.2.: Events before and after selection. The summarized rejection percentage of wjets is calculated with respect to the single weights of the wjets sample.

6. Fitting Background

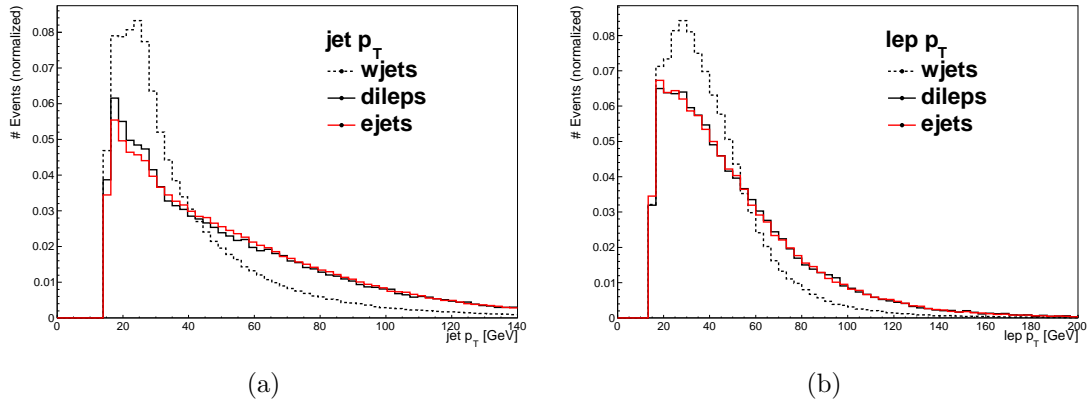


Figure 6.2.: Both distributions are without selection. The p_T distributions of all jets are shown in figure (a). On the right hand side (figure (b)) the p_T distributions of all leptons for signal and background are shown.

6.4. Background Discriminating Variables

As mentioned in the last section the signal to background ratio after the event selection is still smaller than one. The KLFitter reconstructs the $t\bar{t}$ event fully and makes variables accessible for background discrimination, which cannot be measured directly.

Some of these variables are for instance log-likelihood, hadronic or leptonic top mass, the invariant mass of the $t\bar{t}$ -system, the transverse momentum of the $t\bar{t}$ -system and the difference in direction of leptonic b quark and charged lepton, $\Delta R(b_{\text{lep}}, \ell)$. These variables are plotted for all three samples in Figure 6.4. The log-likelihood distribution (6.4(a)) has the highest peak for the ejets sample and has on average higher values than the log-likelihood distribution of the dilep and wjets sample. With this kind of variable it is possible to classify background and signal. For example by choosing $\log L = -30$ as a *decision boundary*. Accepting everything on the right hand side of the cut and rejecting everything on the left hand side, would result in having a lower percentage of background events in the events left as without cut. Of course the total number of signal events decreases.

The top mass distributions are good discriminating variables, as one can see in figure 6.4(b) and 6.4(c). The top mass distributions of the dilep and wjets sample are much broader than the ejets sample. For the wjets sample this is clear because there are no $t\bar{t}$ events in the sample. The reason for the dilep sample is that at least two of the four jets used from the KLFitter to reconstruct the event, are not originating from the four final state quarks of the assumed semileptonic $t\bar{t}$ -decay.

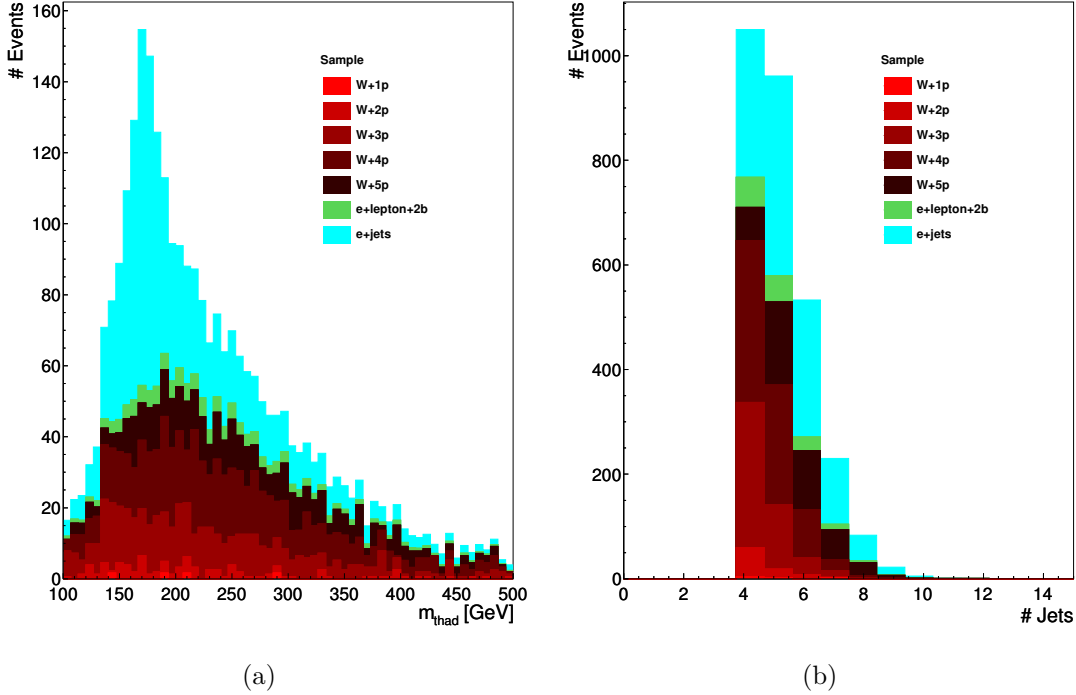


Figure 6.3.: (a) shows the distribution for the calculated top mass of the hadronically decaying top for wjets, dilep and ejets sample. (b) shows the jet multiplicity after selection. In these plots the number of events is not normalized to one and all samples are scaled with respect to their cross sections.

For the plotted variables of the $t\bar{t}$ -system differences between the signal and background samples are observable. There is discriminating potential in the invariant mass (Figure 6.4(d)) distribution, but in the p_T distribution the dilep and ejets sample nearly match (Figure 6.4(e)), resulting in a minor discriminating potential of this variable.

The last of these plots shows the directional difference of the leptonic b quark and the charged lepton. Top-antitop pairs decay into two well separated hemispheres with charged lepton, neutral lepton and leptonic b -jet in the leptonic hemisphere and the other three jets in the hadronic hemisphere. Thus there should be a correlation (smaller ΔR) between the charged lepton and the jet, which the KLFitter assigns to the leptonic b -quark, in the ejets and dilep sample, but not in the wjets sample. As in the wjets sample the charged lepton comes from a W -decay but the W and the jets are not necessarily coming from the same particle, like in the ejets sample, the directional difference should be unrelated. For the dilep sample the

6. Fitting Background

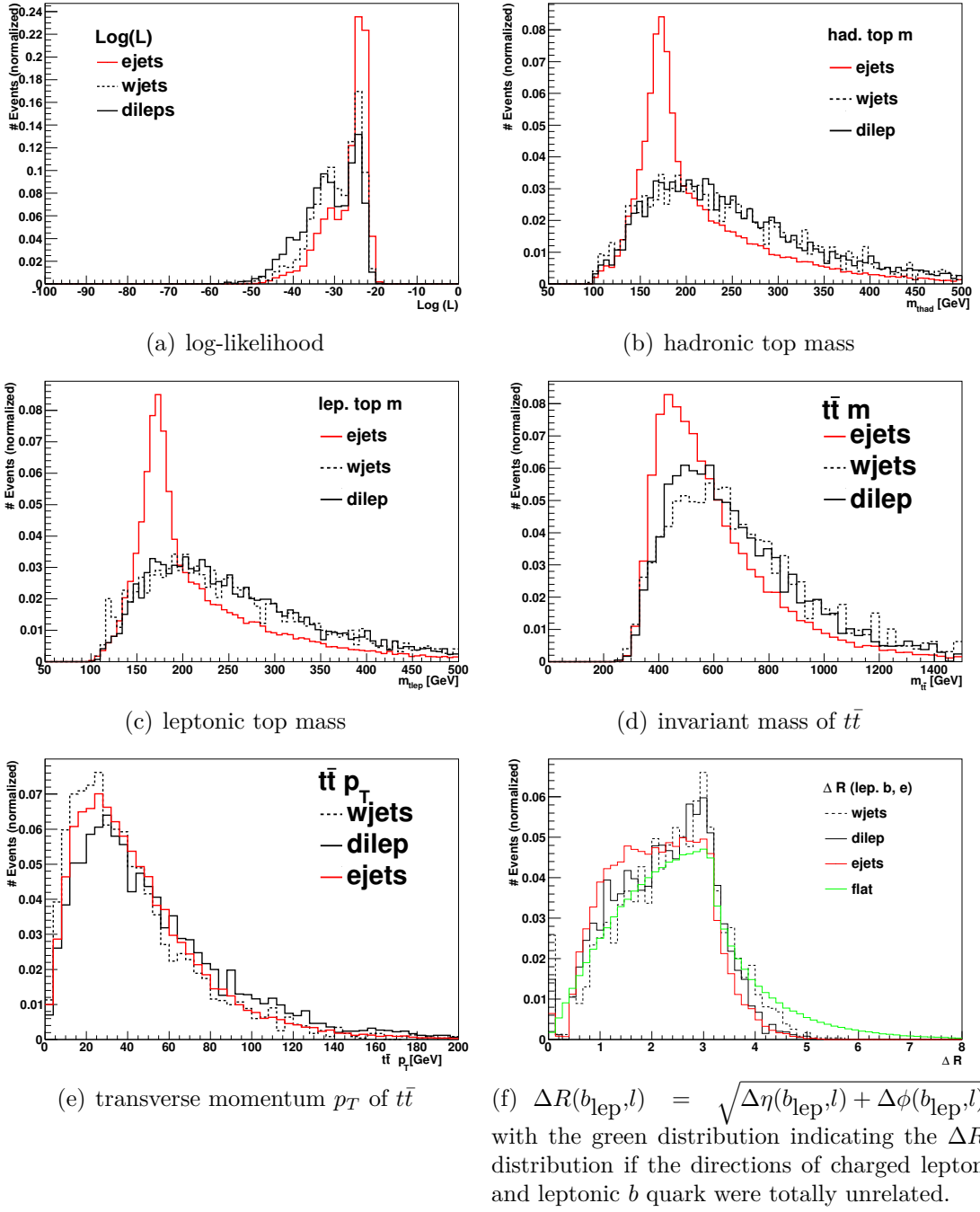


Figure 6.4.: Possible background discriminating variables.

directional difference between the electron and one of the two b -jets should also be small, as they are coming from the same top-quark, but as one b -jet must be labelled as hadronic b -jet by the KLFitter, the probability the KLFitter labels the b -jet as leptonic, which belongs to the selected electron decreases. In Figure 6.4(f) one can observe that the ΔR of the ejets sample is on average smaller than for the other two samples, meaning the charged lepton and leptonic b quark have mostly the same direction. The wjets and dilep sample have a peak at the same value as the *flat* distribution (flat in η and ϕ , cf. figure 6.4(f)), which means the direction of the b quark and charged lepton are mostly uncorrelated. But the dilep sample has still on average a higher ΔR than the wjets sample which is consistent with the mentioned fact, that there are pairs of electron and b -quark coming from the same particle. All these variables have more or less background discriminating potential. With so called *ROC-Curves* (*Receiver operating characteristics*) the discriminating effect of these variables can be quantified.

6.4.1. ROC-Curves

ROC-Curves show the signal efficiency against the background rejection for several cut values. The signal efficiency is defined as the fraction of signal left after the cut, over the total amount of signal without cut. The background rejection is defined as the fraction of background rejected with the cut, over the total amount of background without cut. The plots are produced with a floating cut, meaning one starts with a certain cut value (for instance $\log L = -20$) and moves this cut to a final value. For every single cut the rejection efficiency of background and the signal efficiency are calculated. These ROC-Curves are drawn in figure 6.5. Signal efficiency of one and background rejection of zero (lower right corner) means the cut for this point was done in the way that all events were accepted. The left upper corner shows the signal efficiency and background rejection where the cut was done in the way that all events were rejected. The line dividing the plane is just meant to guide the eye. Cuts creating this kind of ROC-curve would always throw away the same amount of signal and background.

The best cut would be with signal efficiency of one and background rejection of one (right upper corner). Thus ROC-curves reaching closer to the right upper corner can be called best in discriminating signal and background.

6. Fitting Background

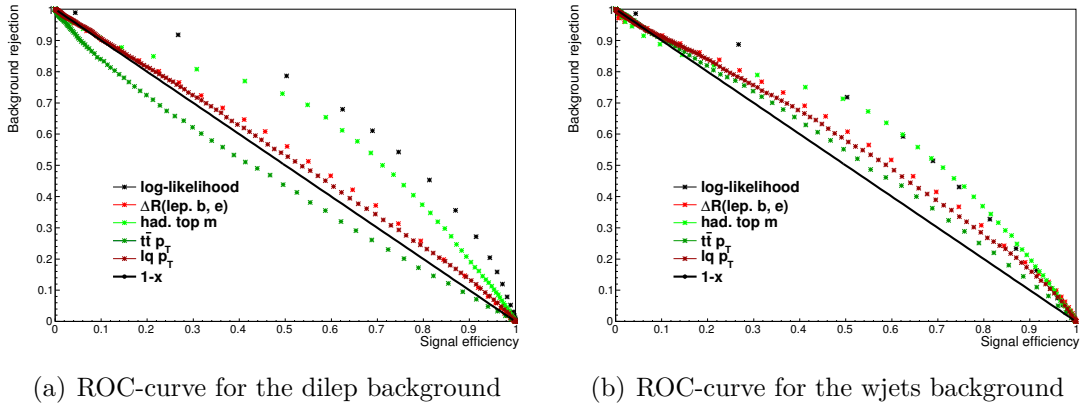


Figure 6.5.: ROC-curves for both background samples.

Looking at Figure 6.5(a) it is obvious that the log-likelihood and the hadronic¹ top mass are the best discriminating variables for the dilep sample. As mentioned before, the number of background events of wjets is higher than the dilep background, thus the discrimination of this background is more important. For the wjets background (Figure 6.5(b)) also the log-likelihood discriminates the background best, but the hadronic top mass does the job as well. The third best discrimination is done by the ΔR variable.

6.4.2. Correlation between different Variables

In Figure 6.6 the correlation between the log-likelihood and the best discriminating variables is visualized, as well as the correlation of log-likelihood and the invariant mass $m_{t\bar{t}}$ of the $t\bar{t}$ -system. In Table 6.3 the linear correlation coefficients are listed. In the Figures 6.6(a), 6.6(d) and 6.6(g) one can observe that the spot with significant filled bins is much smaller for the ejets sample than for the respective figures of the wjets and dilep sample. This means the background samples are flatter in these parts of phase space.

Examining the correlation plots of the signal one can observe that they make sense: In Figure 6.6(a) one can observe that the peak in every $\log L$ -slice is at smaller ΔR values, with increasing $\log L$. This anti-correlation makes sense as high $\log L$ indicates good reconstruction of an event and ΔR of $t\bar{t}$ -events is expected to be small. Also figure 6.6(g) makes sense as events with a reconstructed top mass of

¹Of course there is no hadronic top quark in the dilep sample, but the KLFitter fits always with the assumption having one hadronic and one leptonic top quark. Therefore it exists a hadronic top quark in the fitted sample.

172.5 GeV should come with a high $\log L$.

The lowest linear correlation in all three variable combinations have $\log L$ and ΔR . Because of this fact, cutting on both these variables the most background rejection for a certain signal efficiency should be possible. The aim is to find two variables which have a low correlation for the background, because then it can be expected that cuts on the first variable affects other events than cuts on the second variable.

Correlation of $\log L$ to	ejets	dilep	wjets
$\Delta R(b_{\text{had}}, \ell)$	-30.4 ± 0.4	-11.2 ± 1.1	-17.7 ± 2.0
$m_{t\bar{t}}$	-33.4 ± 0.4	-36.8 ± 1.0	-33.1 ± 1.9
$m_{t\text{had}}$	-51.9 ± 0.3	-42.2 ± 0.9	-42.1 ± 1.7

Table 6.3.: Linear correlation factors of $\log L$ with three other variables for the signal and background samples. All numbers in %. The errors, σ , were calculated with the approximation formula $\sigma = (1 - \rho^2)/\sqrt{N - 1}$, with ρ the linear correlation and N the number of events [15, p. 80].

6.4.3. Exemplary Cuts

As exemplary cuts, the rejection of all events with $\Delta R(b_{\text{lep}}, \ell) > 2.2$, the rejection of those events with $\log L < -26$ and the combined cut of rejecting all events with $\Delta R(b_{\text{lep}}, \ell) > 2.2$ or $\log L < -26$ are examined. These values are chosen in the way that after the cuts more than 50% of signal is left. The efficiencies² for all three cuts are listed in Table 6.4.3. Only percentages are given, as the number of events has to be scaled by the appropriate cross section to be comparable. Regarding only the

Cut	ejets	dilep	wjets
ΔR	52.6 ± 0.3	46.4 ± 1.0	41.8 ± 2.4
$\log L$	57.6 ± 0.3	27.8 ± 1.1	35.5 ± 2.5
combined	35.6 ± 0.5	14.8 ± 1.2	17.5 ± 2.8

Table 6.4.: Absolute efficiencies of the exemplary cuts of $\Delta R(b_{\text{lep}}, l) > 2.2$, $\log L < -26$ and the combined cut. All values in % and with binomial errors.

percentages, the $\log L$ -cut is more efficient than the ΔR cut for both backgrounds. Define the goodness of a cut as ratio of the percentage of kept signal over the

²percentage of accepted events

6. Fitting Background

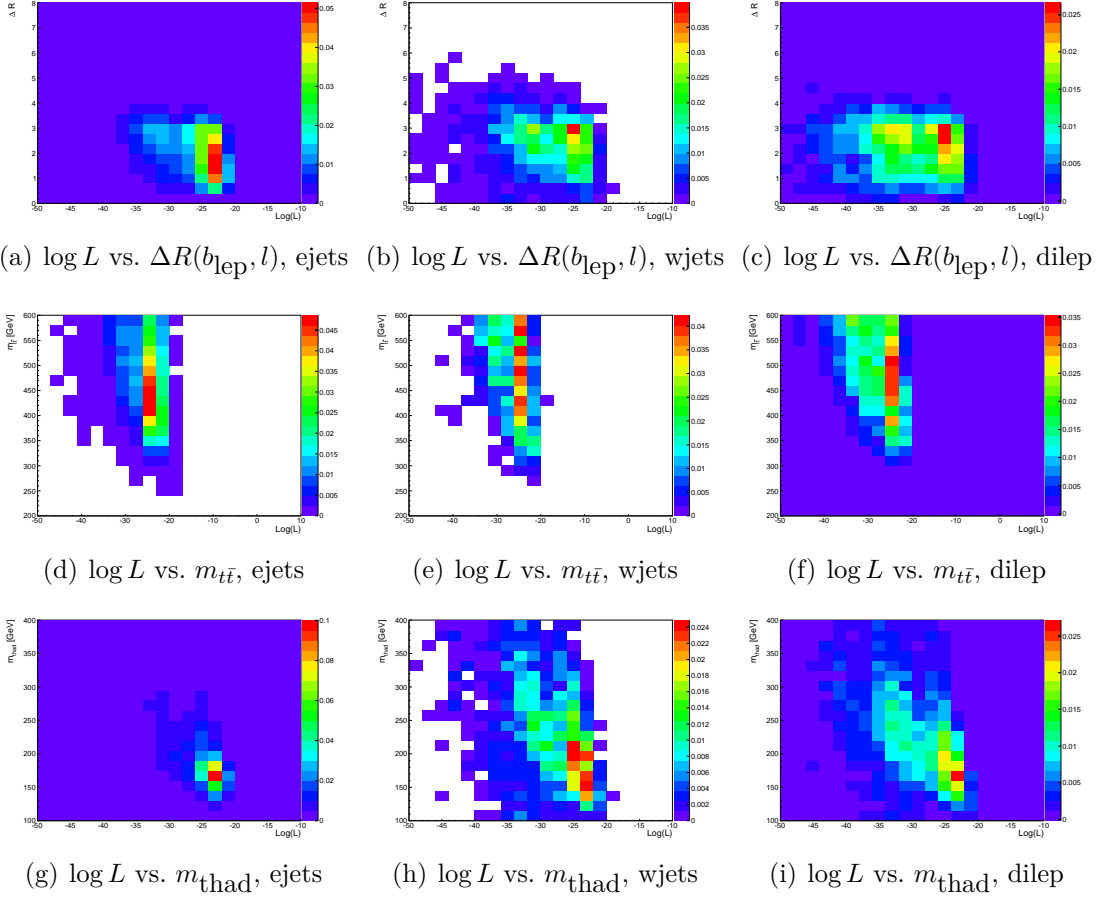


Figure 6.6.: Two dimensional histograms of log-likelihood with three other variables to study the correlation of these variables in all three samples. All plots are normalized to 1.

percentage of kept background ($g(\text{cut}, \text{background sample})$).

$$\begin{aligned} g(\Delta R, \text{dilep}) &= 1.13, \\ g(\Delta R, \text{wjets}) &= 1.26, \\ g(\log L, \text{dilep}) &= 2.08, \\ g(\log L, \text{wjets}) &= 1.63, \end{aligned}$$

This is of course consistent with the ROC-curves in section 6.4.1, as they motivated these exemplary cuts.

The cut flow is not the only criterion for a useful cut to separate signal from background and therefore some kinematic distribution will be examined after a cut was performed. An efficient cut can only be called “useful” if additionally the following points hold.

In an ideal case the rejected signal should be evenly distributed over the left phase-space³. Otherwise any analysis on the remaining signal events would probably be biased and suffer from systematic errors.

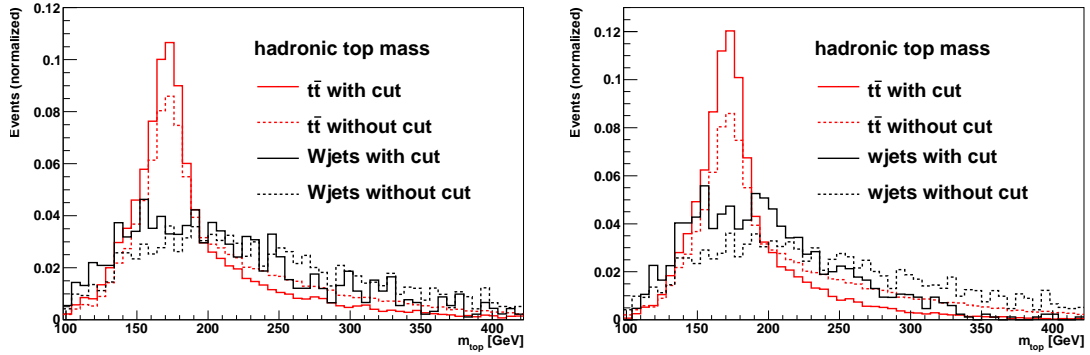
If two cuts reject the same amount of events, the one after which the background is still distinguishable in some variable is “more useful” than the other. Hence, another cut can be used to discriminate the background from the signal. Also template fits can only be performed to estimate the background contribution on a sample which contains an unknown part of background, if both distributions are distinguishable. In the following, it will be studied to which degree the background resembles the signal after a performed cut. The cuts are examined for both background samples separately.

Cuts on Wjets Sample

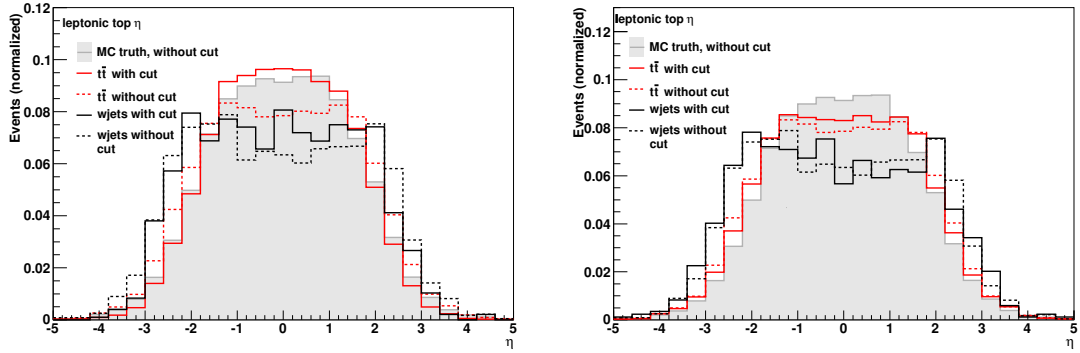
The mentioned cut on ΔR and $\log L$ show an improvement of the top mass distributions (see Figure 6.7(a) and 6.7(b)) for signal. In both plots the peak heights increase and the position of the peak does not change. This means that the hadronic top mass matches the truth value better with the cut applied. The same holds for the leptonic top mass shown in the Appendix B. The top mass distribution of wjets background behaves similarly under the cuts, the peak height increases. Its mean becomes lower, because more events with high invariant masses are rejected. This effect can in particular be seen in the hadronic top mass distribution with the $\log L$

³The phase-space spanned by variables, on which no cut was performed

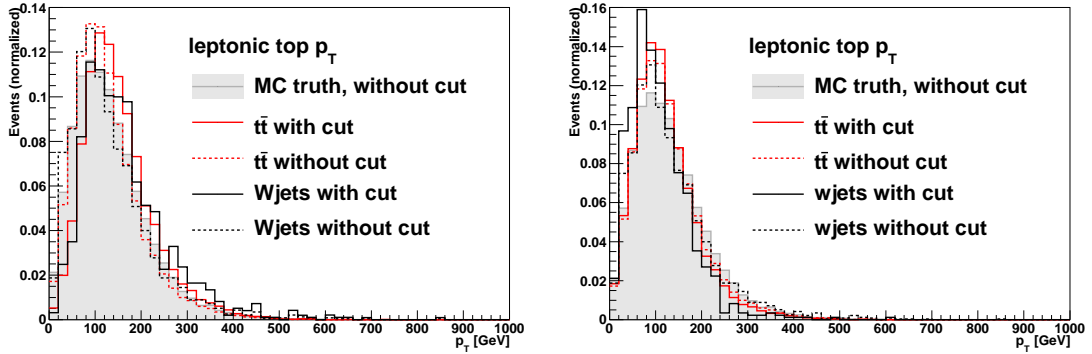
6. Fitting Background



(a) hadronic top mass with and without ΔR cut (b) hadronic top mass with and without $\log L$ cut



(c) leptonic top η with and without ΔR cut (d) leptonic top η with and without $\log L$ cut



(e) leptonic top p_T with and without ΔR cut (f) leptonic top p_T with and without $\log L$ cut

Figure 6.7.: Selected distributions of signal (ejets) and background (wjets) with and without cut.

cut. As the log-likelihood is strongly anti-correlated with the top mass (see Table 6.3) rejecting events with low log-likelihood means rejecting events with high top masses. But still the background distribution is much broader than the signal distribution.

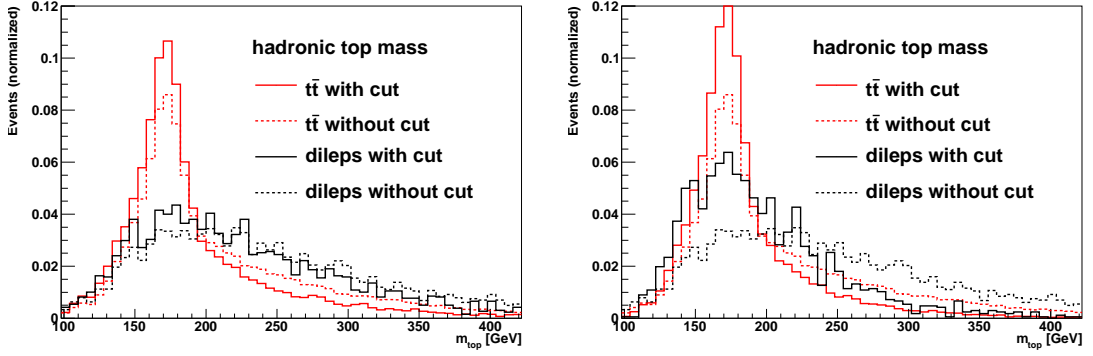
Figures 6.7(c) and 6.7(d) show the η -distribution of the leptonic top with underlying truth distribution. One observes that with the ΔR -cut the signal matches the truth distribution very well. The same effect is visible for the log L -cut, but not as strong as in the ΔR -cut. On the other hand the wjets background is before and after both cuts visibly broader than the truth and the signal distribution. The ejets top η distribution has a standard deviation of $\sigma = 1.58$ which reduces to $\sigma_{\Delta R} = 1.38$ (ΔR -cut) and $\sigma_{\log L} = 1.54$ (log L -cut), while the wjets top η distribution has $\sigma = 1.79$ which reduces in the ΔR -cut to $\sigma_{\Delta R} = 1.65$ but increases to $\sigma_{\log L} = 1.81$ in the log L -cut. This means with both cuts the wjets background can still be discriminated from the signal in the η -distribution. The wjets background resembles the hadronic top mass distribution of the signal more after the log L -cut than after the ΔR -cut. But in the part of phase space shown in the top η -distribution it looks less like signal after the log L -cut.

Figures 6.8(e) and 6.8(f) show the transverse momentum distribution of the leptonic top. Without cuts, signal and wjets background match approximately, also they follow the MC truth distribution, except for the peak position. When the ΔR -cut is applied, the signal and the background distribution are shifted to higher p_T . This means the ΔR -cut rejects mainly events with low p_T . Also the background p_T distribution matches the truth in the region of the peak better than the signal distribution does. For high p_T , the signal matches the truth distribution better than the background. Signal and background reproduce the truth distribution worse.

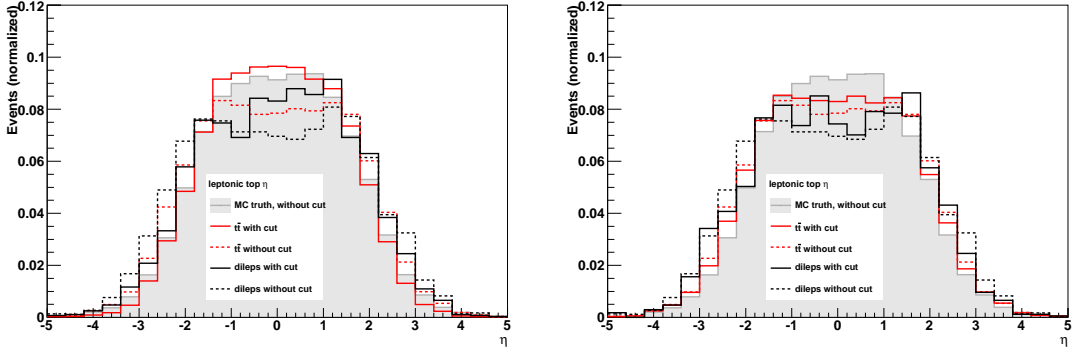
The log L -cut behaves better, as there is no huge difference between the signal distribution with and without cut (Figure 6.8(f)). For the background distribution there is a clearly visible shift to lower p_T . But in the end the background discriminating effect of top p_T is not as high, as of top η .

The conclusion is that wjets is still distinguishable in the η - and top mass distributions after both cuts. There is no systematic shift of the top mass peak for the signal. But the ΔR cut shifts p_T systematically.

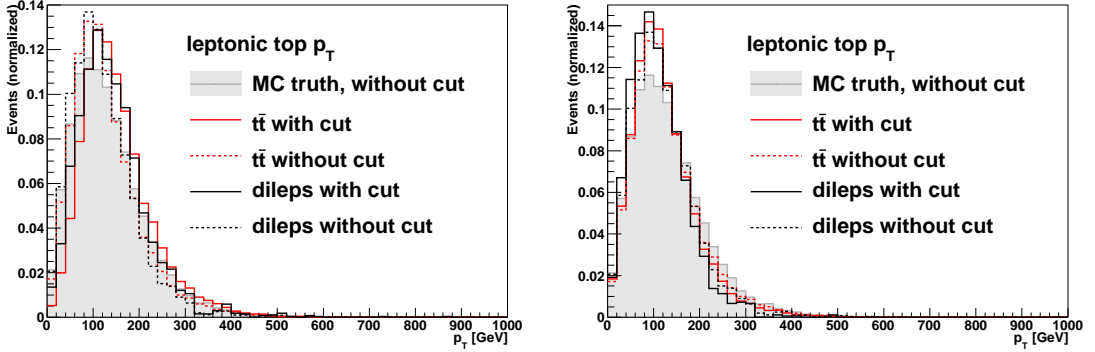
6. Fitting Background



(a) hadronic top mass with and without ΔR cut (b) hadronic top mass with and without $\log L$ cut



(c) leptonic top η with and without ΔR cut (d) leptonic top η with and without $\log L$ cut



(e) leptonic top p_T with and without ΔR cut (f) leptonic top p_T with and without $\log L$ cut

Figure 6.8.: Selected distributions of signal (ejets) and background (dilep) with and without cut.

Cuts on Dilep Sample

The hadronic top mass distributions of the dilep and the wjets sample are comparable without cuts (both are broad with respect to the ejets sample, see Figure 6.8 and 6.7). Also after the ΔR -cut (Figures 6.8(a)), the hadronic top mass distribution of dileptonic events is as flat as the distribution of wjets events. But after the $\log L$ -cut the top mass distribution forms a clearly visible peak (Figure 6.8(b)).

The difference of dilep events in the leptonic top η distribution to ejets events is not as distinct as for wjets events (Figure 6.8(c) and 6.8(d)). Also the dilep sample matches the truth top η distribution with both cuts better than without, which is not the case for the wjets sample.

After cutting on ΔR , the shift to higher p_T values for the dilep sample is visible but not as distinct as for the wjets sample (Figures 6.8(e) and 6.7(e)). Furthermore the dilep distribution matches the signal distribution before and after the ΔR cut without huge deviations. The same holds for the distributions of dilep and ejets before and after the $\log L$ cut.

Generally the dilep sample matches the ejets sample better than the wjets sample does. Also cutting on ΔR and $\log L$ leaves in the dilep sample more events which look like signal than in the wjets sample. This means it is easier to discriminate wjets background from signal than dilep background.

Combined Cut

The combination of the two cuts ($\log L$ and ΔR) rejects about 64% of signal events, 82% of wjets background and 85% of dilep background events. This results in the hadronic top mass distribution shown in Figure 6.9. The left dilep and wjets events from samples with less than 3 partons are negligible.

Figure 6.10(a) and 6.10(b) show that after the combined cut the wjets and dilep backgrounds form a broad peak around the true top mass. Also the mean of the peak region for the signal shifts to lower top masses. In the top η distributions the wjets background is still distinguishable from the signal distribution, whereas the dilep background matches the signal distribution after the combined cut and truth distribution (see Figures 6.10(c) and 6.10(d)). The last two figures (6.10(e) and 6.10(f)) show the invariant mass of the $t\bar{t}$ system before and after the combined cut. One observes that the combined cut shifts the background distributions in the direction, that they match the truth MC and signal distribution better than

6. Fitting Background

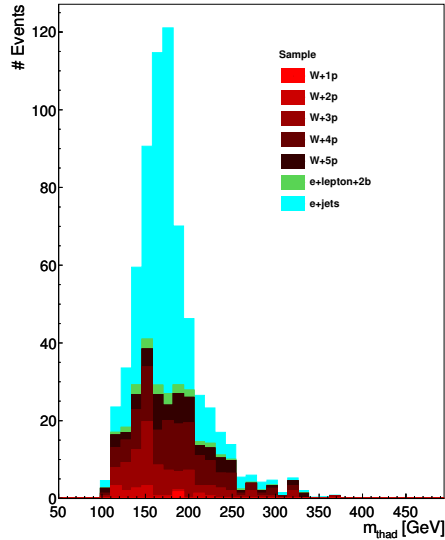


Figure 6.9.: Hadronic top mass distribution of wjets, dilep background and signal, scaled to reflect the cross sections.

without cut. The combined cut rejects mainly events with high invariant mass of $t\bar{t}$. But the peak of the distribution increases more strongly for the signal than for the background.

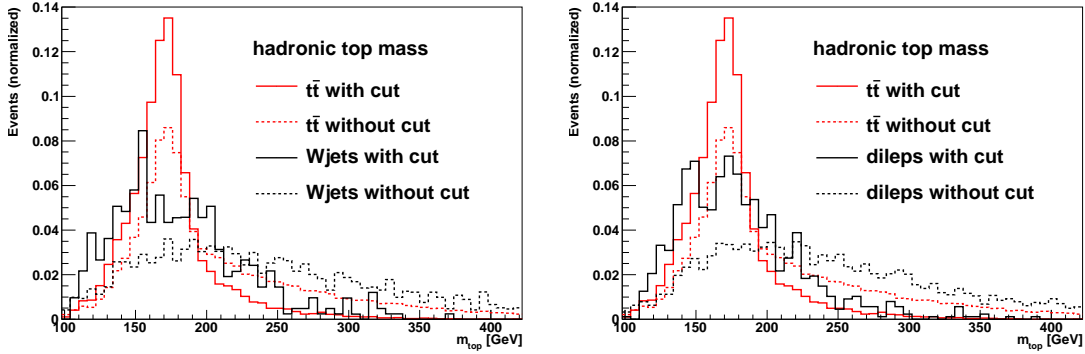
After the combined cut the dilep background looks more like the signal as the wjets background does, but the contribution of the dilep background to the total amount of background is negligible. Therefore only wjets background is considered in the next section.

6.5. Fitting five Jets

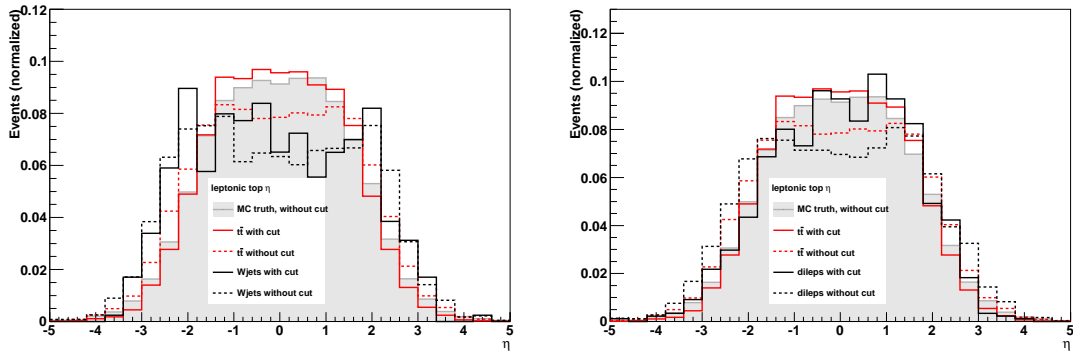
In the last sections the results were obtained by selecting events with a minimum of 4 jets and then selecting the 4 jets with highest p_T . This leads to 12 possible jet to quark mappings, meaning the KLFitter performs 12 fits for every event.

In this section, the background discriminating effect of the log-likelihood will be studied, if one selects 5 jets instead of 4. Now the KLFitter is operated in a different mode. The same events are selected as before, but if there are 5 jets, the KLFitter takes 5 jets and tries to find the right jet-to-quark combination. Thus here the considered operating mode of the KLFitter is: if possible fit 5 jets, otherwise fit 4 jets.

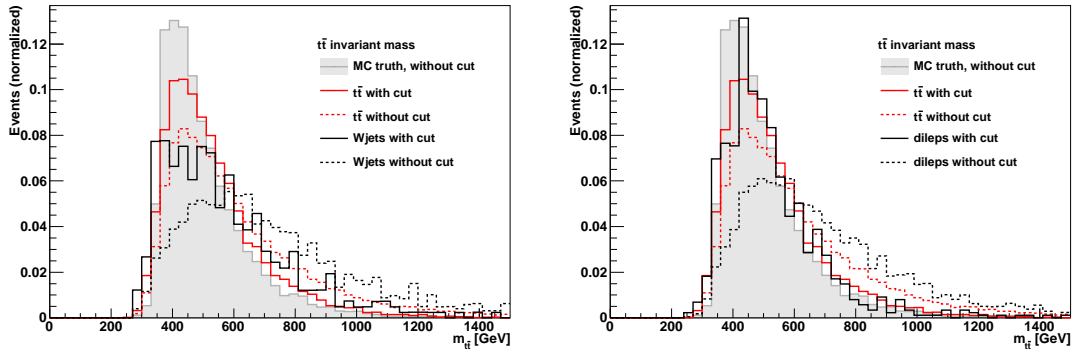
Selecting 5 jets as candidates for the 4 quarks increases the possible jet-to-quark



(a) hadronic top mass with and without cuts of ejets and wjets (b) hadronic top mass with and without cuts of ejets and dilep



(c) leptonic top η with and without cuts of ejets and wjets (d) leptonic top η with and without cuts of ejets and dilep



(e) leptonic top $t\bar{t}$ invariant mass with and without cuts of ejets and wjets (f) leptonic top $t\bar{t}$ with and without cuts of ejets and dilep

Figure 6.10.: Selected distributions of signal (ejets) and background (wjets on left hand side, dilep on right hand side) with and without combined cut.

6. Fitting Background

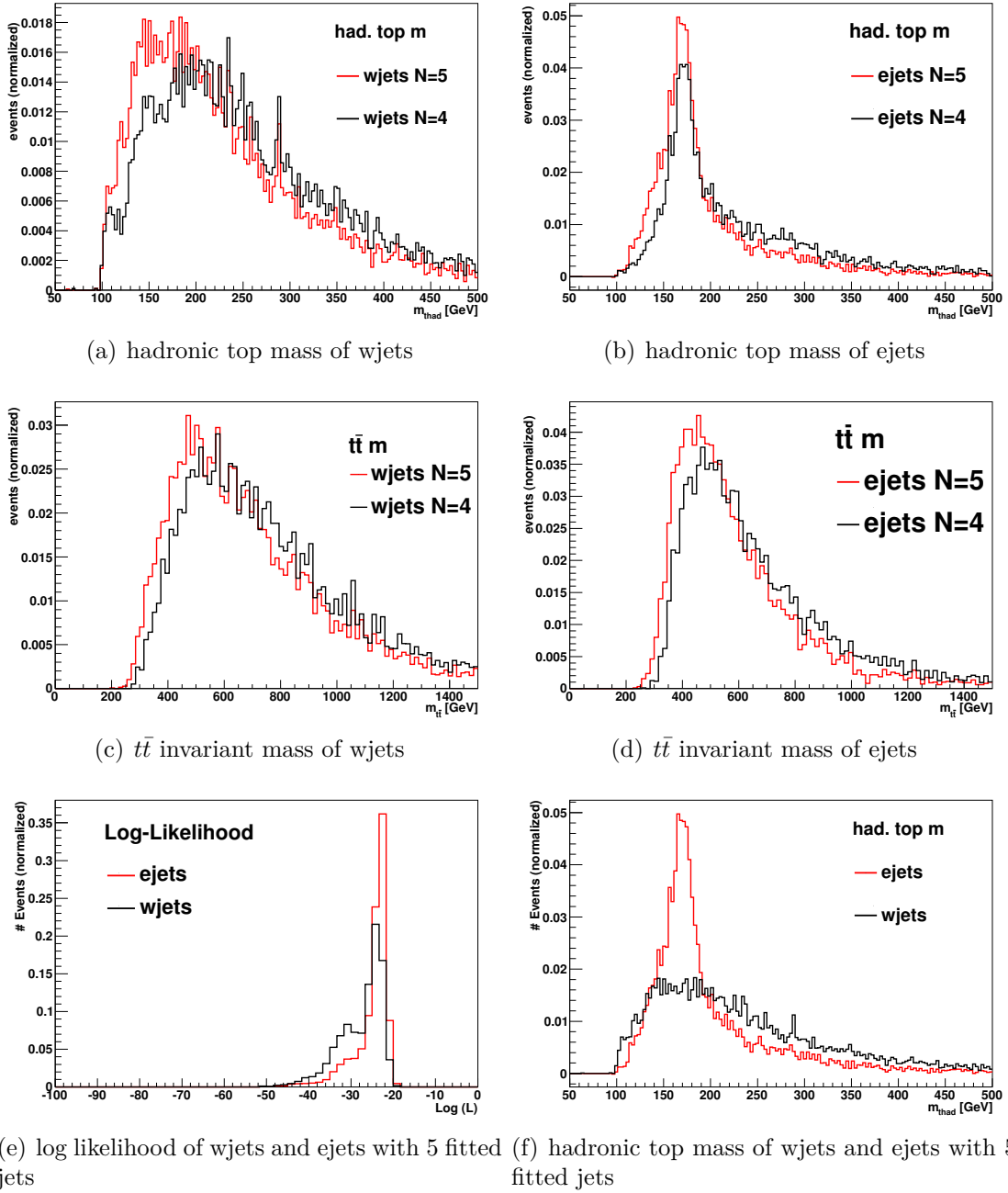


Figure 6.11.: Comparison of some exemplary distributions after fitting 5 jets (if possible) instead of 4 with the default operation mode of the KLFFitter (fitting 4 jets).

mappings to 60. This means that the number of fits the KLFitter performs is 5 times higher as before and thus slows down the program significantly. On the other hand the possibility increases that within the 5 jets there are the 4 jets originating from the 4 truth quarks.

One defines the matching efficiency ε_m as number of all selected events in which the selected jets could be matched uniquely to the 4 truth quarks (truth matching⁴) divided by the number of events considered.

The reconstruction efficiency ε_r is based only on matched events (see Section 5). One takes all matched events and calculates the percentage of those events which are reconstructed in the true jet-to-quark combination. Since drawing the right combination out of 60 is less probable than drawing from 12, the reconstruction efficiency decreases⁵ if one uses 5 instead of 4 jets to fit.

To reconstruct an event in the right way, there have to be the four jets originating from the truth quarks under the five (four) selected jets. Additionally the KLFitter has to select the right combination out of the 60 (12) possibilities. This explains the definition of the *total reconstruction efficiency*, ε , as product of the matching and the reconstruction efficiency: $\varepsilon = \varepsilon_m \cdot \varepsilon_r$. The matching increases with increasing number of fitted jets, whereas the reconstruction efficiency decreases with increasing number of fitted jets. Disregarding any systematic effects arising from fitting more than four jets, the optimum can be found [21] by fitting 5 jets, if possible. For the ejets sample used in Figure 6.11 the efficiencies are listed in table 6.5.

fitted jets	ε [%]	ε_m [%]	ε_r [%]
4	13.2 ± 0.6	24.0 ± 0.9	55.2 ± 1.3
5	15.8 ± 0.5	38.7 ± 0.8	40.8 ± 0.9

Table 6.5.: Improvement of total reconstruction efficiency if 5 jets are fitted (if possible) instead of just 4 jets in the signal sample (ejets).

Figure 6.11(a) to (d) show a systematic shift to lower top masses, if the sample is fitted with 5 jets. But the peak heights increase mainly for the ejets distribution, but not so much for the wjets background distribution. This indicates, that discriminating background and signal could be easier if 5 jets are fitted. Figure 6.11(f)

⁴see end of Chapter 4.2.1 and beginning of Chapter 5

⁵Of course this explanation is valid only, when drawing randomly and the KLFitter does not draw combinations randomly out of all possible combinations. But this “worst case” approximation of the KLFitter intuitively explains the results in Table 6.5

6. Fitting Background

shows that the background is still broad with respect to the signal in the hadronic top mass distribution. The $\log L$ distribution is again used to create a ROC-curve to examine the discriminating effect of the log-likelihood, if 5 instead of 4 jets are fitted. The ROC-curve comparison in Figure 6.12 shows that the wjets background

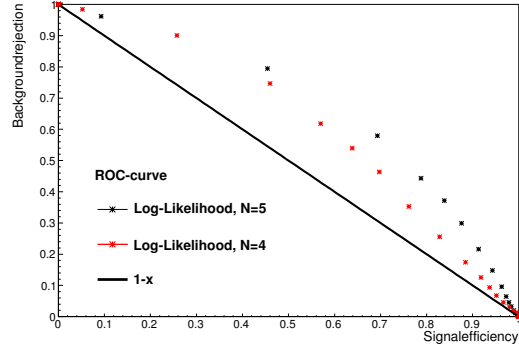


Figure 6.12.: Comparison of ROC-curves of log-likelihood if fitting was done with 4 or 5 jets.

discrimination of $\log L$ is stronger if 5 instead of 4 jets are fitted. Uncertainties coming from the MC generator affect the fifth jet more than the other four, because a fifth jet only arises if effects like ISR, FSR, etc. occur and these effects are probably not well described in the MC generator. Thus the improvement of the discriminating effect could be⁶ a systematic effect introduced by the MC generator.

⁶but not expected

7. Comparison of two Sets of Transfer Functions

In this section the performance of the fitter with two different sets of transfer functions (TF) are examined. For this comparison a $t\bar{t} \rightarrow \mu + \text{jets}$ sample is used. The principal difference of both sets of TFs (called *NewTF* and *OldTF*) is, that the OldTF-set contains as TF for muon p_T a simple Gaussian function (Section 4.3) with one extracted parameter (the width) for all η -ranges, whereas the NewTF-set contains a double Gaussian TF with ten extracted parameters a_i for three different η -ranges:

$$W(\tilde{p}_T|p_T) = \frac{1}{\sqrt{2\pi}} \cdot \frac{1}{\sigma_1 + m \cdot \sigma_2} \left(\exp\left(-\frac{(\Delta p_T - \mu_1)^2}{2\sigma_1^2}\right) + m \exp\left(-\frac{(\Delta p_T - \mu_2)^2}{2\sigma_2^2}\right) \right),$$

the symbols are defined as follows

$$\begin{aligned} \mu_1 &= a_1 + p_T \cdot a_2, \\ \sigma_1 &= a_3 + p_T \cdot a_4, \\ m &= a_5 + p_T \cdot a_6, \\ \mu_2 &= a_7 + p_T \cdot a_8, \\ \sigma_2 &= a_9 + p_T \cdot a_{10}, \\ \Delta p_T &= \frac{p_T - \tilde{p}_T}{p_T}. \end{aligned}$$

Moreover, the sample which was used to extract the parameters for the NewTF-set is the same on which the TF comparison is done, the OldTF-set was extracted on a different sample. For the comparison of both TF-sets, the matching of the fitted data with MC truth (Figure 7.1) and afterwards the energy resolution of the transfer functions (Figure 7.2) are examined. The first plots show large differences in the results of the KLfitter for both sets of transfer functions. One can see that the broadness of the leptonic top η -distribution of the NewTF-set matches the MC truth

7. Comparison of two Sets of Transfer Functions

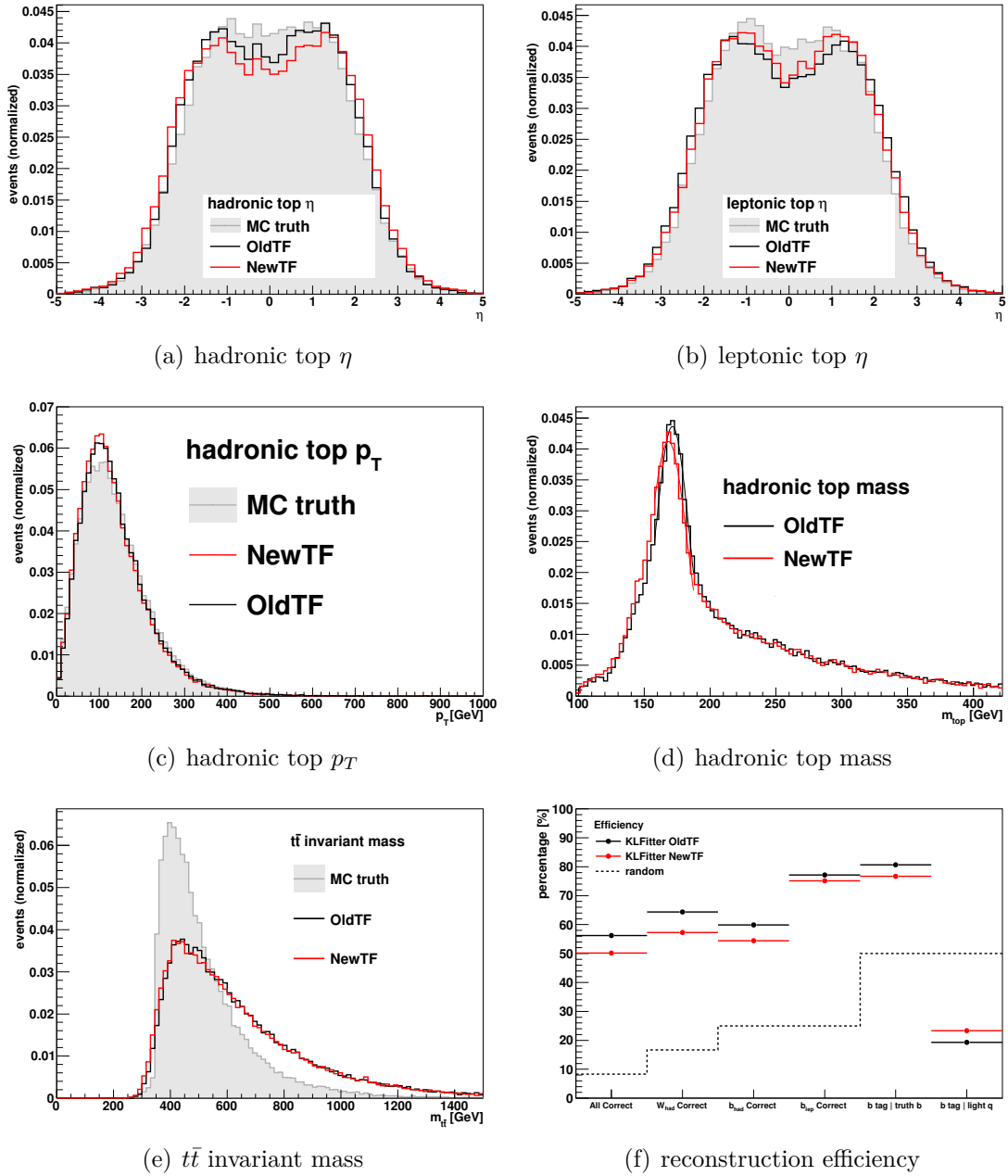


Figure 7.1.: Comparison of the results of KLFitter when using two different sets of transfer functions (NewTF and OldTF).

energy resolution of	mean (OldTF)	mean (NewTF)	width (OldTF)	width (NewTF)
hadronic b quark	0.13 ± 0.15	-0.11 ± 0.18	1.19 ± 0.24	1.25 ± 0.25
leptonic b quark	0.24 ± 0.13	-0.01 ± 0.10	1.23 ± 0.17	1.22 ± 0.19
light quarks	0.25 ± 0.17	0.19 ± 0.12	0.81 ± 0.21	0.81 ± 0.33

Table 7.1.: Fit values for the Gaussian fit of the central range of the energy resolutions. All values in units of $\text{GeV}^{1/2}$.

sample better than the OldTF-set. But the opposite effect can be observed for the hadronic top η -distribution. Figure 7.1(c) and 7.1(d) show also a negative behaviour of the NewTF-set compared to the OldTF-set. The peak of the hadronic top mass shifts to lower masses, away from the ideal peak at 172.5 GeV. Additionally, the peak height drops, which means that the distribution for the NewTF-set is broader than for the OldTF-set.

The $t\bar{t}$ invariant mass (Figure 7.1(e)) does not match the MC truth distribution for both TF-sets. Also the reconstruction efficiencies decrease significantly when using the NewTF-set. All plots are taken from the output of a $\mu + \text{jets}$ -sample, but the same results can be observed when an $e + \text{jets}$ sample is used (see Appendix C).

The resolution plots (Figure 7.2) show partly an opposite effect, as one can observe (for the b -jet and light quark energy resolution) that the mean of the peak is closer to zero for the NewTF than for the OldTF-set (see also Table 7.1). The light quark energy resolution can not be calculated for each light quark separately, because they are indistinguishable for the KLFitter and thus it is not known if the quark labeled from the KLFitter as light quark 1 originates from the truth light quark 1 or 2. Therefore the energy resolution of the sum of both light quark energies is considered here. On the other hand the energy resolutions are broader for the NewTF-set than for the OldTF-set, even if the width of the central Gaussian fit shows no significant difference between NewTF- and OldTF-set.

After examining these performance plots, one observes that the NewTF-set shows significantly better results for the variables based on the reconstruction of the muon, but all variables which do not need directly the four vector of the muon (i.e. hadronic top mass, hadronic top η etc.) show better results with the OldTF-set. The energy resolution plots indicate a slight improvement with the NewTF-set but the kinematic plots and efficiencies are not satisfying. One needs to study the behaviour of the KLFitter with different sets of transfer functions in more detail, to obtain more reliable conclusions on this matter.

7. Comparison of two Sets of Transfer Functions

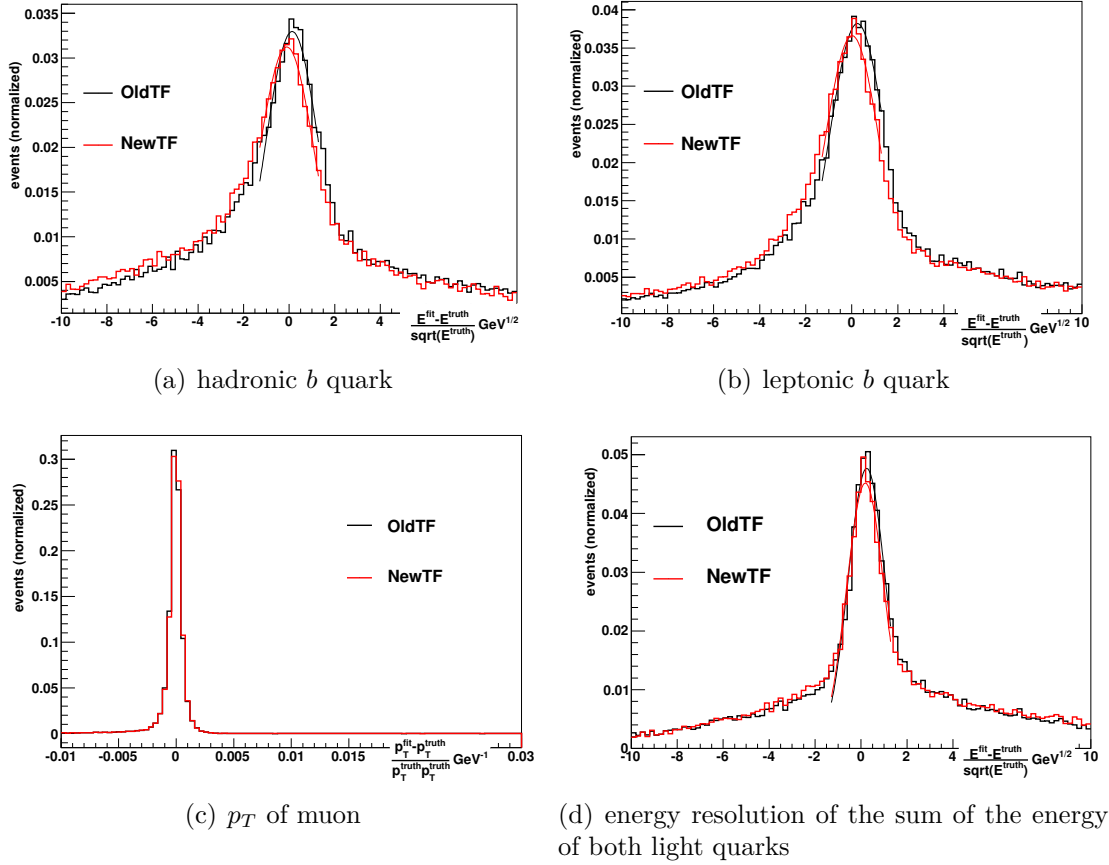


Figure 7.2.: Energy resolution of quarks and transverse momentum resolution of muons.

8. Conclusion

In this bachelor thesis, MC generated $t\bar{t}$ decays with e +jets and μ +jets final states were studied with a kinematic fitter (the KLFitter). In Chapter 5 it was shown that the KLFitter reconstructs kinematics of the top quark in general equally well for e +jets and μ +jets events. Slightly better results were observed for the μ +jets sample, actually. One point to mention is, that for μ +jets the transfer function used for the muon momentum, has only one parameter, whereas the transfer function for the electron energy used for e +jets has ten parameters for three different η -ranges. Because of this observation, the performance of the KLFitter was studied with different sets of transfer functions in Chapter 7. This study shows that a more precisely extracted muon transfer function may improve those results of the KLFitter which depend directly on the reconstruction of the muon. Also, this study shows that the output of the KLFitter is mainly independent of the choice of both studied sets of transfer functions and it cannot be concluded that one set is better than the other from this study.

The main part of this thesis addresses the behaviour of w jets and dilep background when fitted with the KLFitter. It was shown in the first part of Chapter 6 that the most part of these two background contributions is rejected with the event selection, which increases the signal to background ratio.

Afterwards a number of variables, which are only accessible after the reconstruction of the full decay topology, were studied. They have additional potential to discriminate signal from background. It turned out that $\log L$ is the best discriminating variable of the studied ones.

Three exemplary cuts ($\log L < -26$, $\Delta R(\text{lep}, b, e) > 2.2$, and the combination of both cuts) were applied on signal and background and the resulting kinematics were examined for systematic effects. It was shown that w jets background looks less like signal than the dilep background after applying the cuts. Also the ΔR -cut leads to stronger shifts in the p_T distributions than the $\log L$ -cut. The combined cut shows a systematic shift to lower top masses of the signal. Also the combined cut showed

8. Conclusion

that it is possible to rise the signal to background ratio above one with very simple cuts. This means that even if the W +jets background is called *irreducible* as the topology of these events is equal to the signal topology, it is possible to discriminate huge parts of this background, first with directly accessible variables like p_T of jets and lepton and secondly with variables accessible through full reconstruction of all events like $\log L$, ΔR and top mass.

The fact that this is possible, means also that the background behaves differently under the kinematic fitting with the ML method. This leads to the fact that wjets background after the fitting procedure is still distinguishable from the signal, although the fitter tries to interpret the events as signal events.

Moreover, the possibility of fitting 5 instead of 4 jets was studied. Fitting in this mode increases the background discriminating effect of $\log L$, because the peak of log-likelihood rises for the signal more than for the wjets background. But as already mentioned fitting 5 instead of 4 jets increases the possibility that this observed improvement is a systematic effect coming from the MC generator.

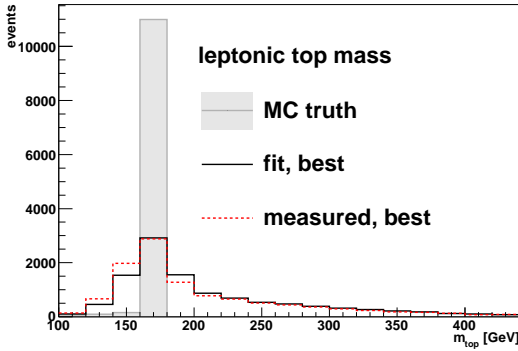
8.1. Outlook

As for the TF-study all TFs in both TF-sets were different, a more simplified study should explain the behaviour of the KLFitter under different TFs.

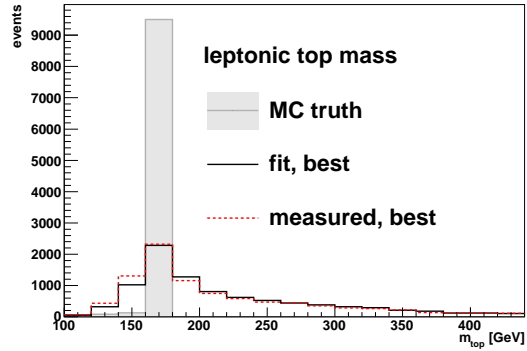
Regarding the background discrimination-part of this study, there are more sophisticated methods to discriminate background from signal, like the TMVA-package integrated in ROOT, based on neuronal networks to make nonlinear cuts in the space spanned by many discriminating variables, but this is a first step to decide whether some variables are useful to cut on or not.

9. Appendix

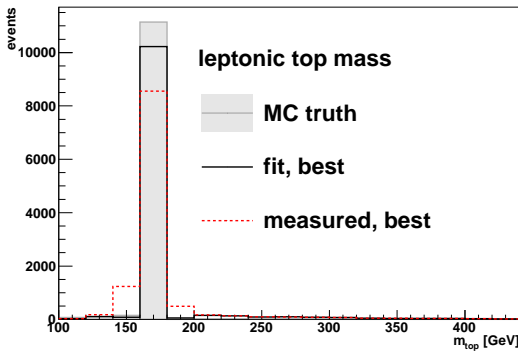
A. Fitting muon+jets Final States



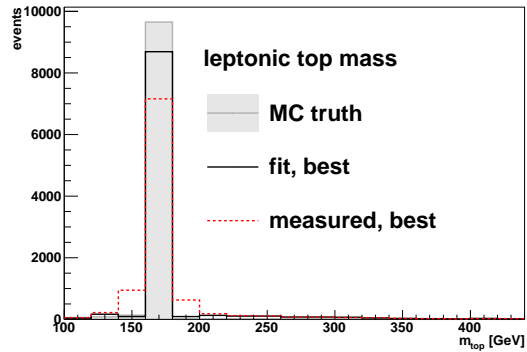
(a) μ +jets sample with free top mass



(b) e +jets sample with free top mass



(c) μ +jets sample with fixed top mass



(d) e +jets sample with fixed top mass

Figure A.1.: Comparison of e +jets and μ +jets sample with leptonic top mass distribution.

The leptonic top mass distributions show the same qualitative characteristics as the hadronic top mass distributions discussed in Chapter 5. In the plots (Figure 9.1(a) and 9.1(b)) the fitted distributions have nearly the same heights as the MC truth “distributions”, what is not so much the case for the hadronic top masses. This is consistent as it is easier to reconstruct the leptonic hemisphere.

9. Appendix

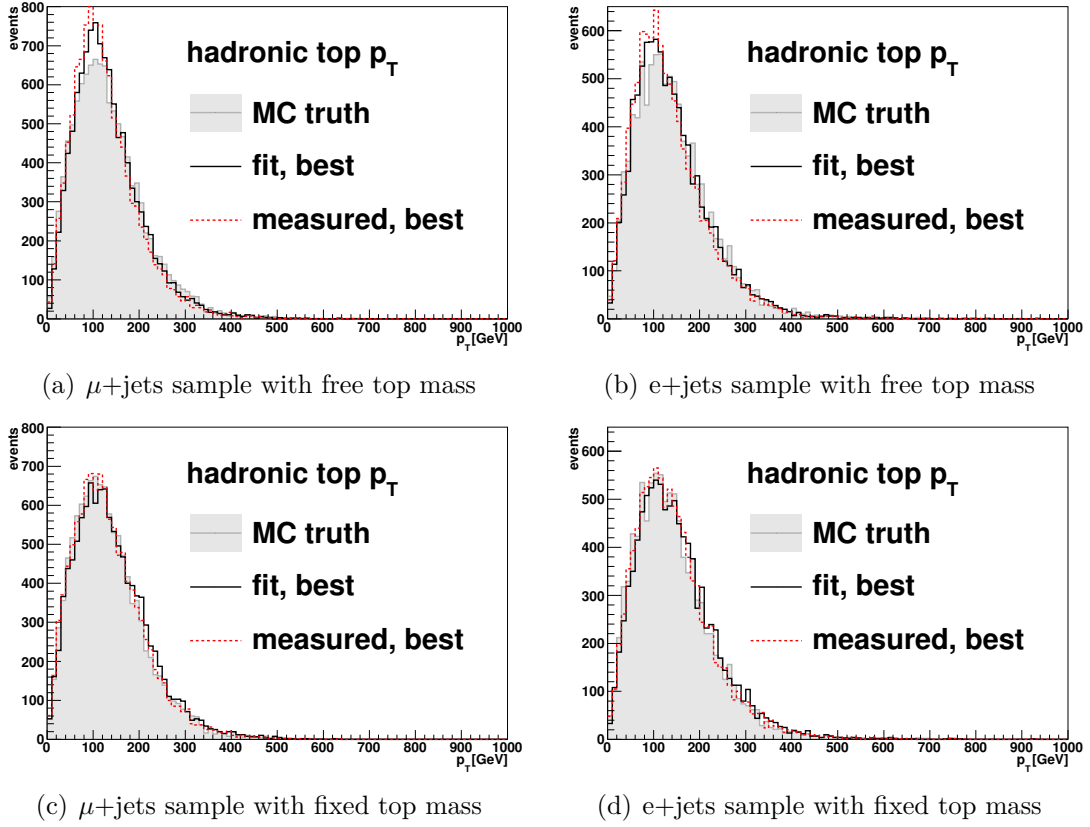
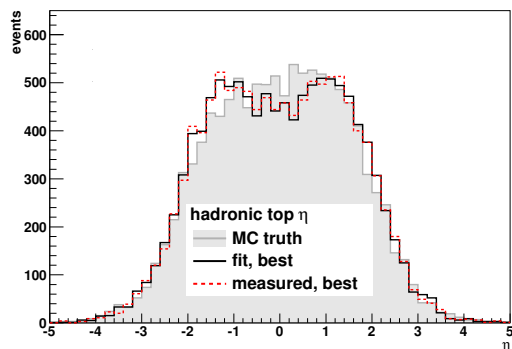
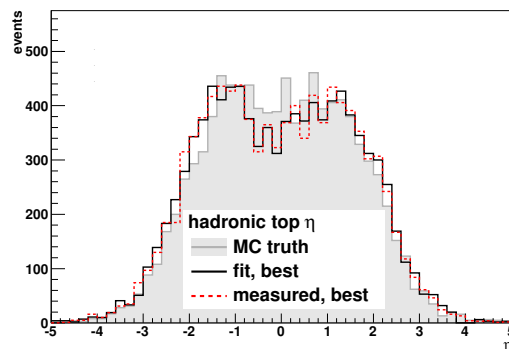


Figure A.2.: Comparison of e +jets and μ +jets with hadronic top p_T distribution.

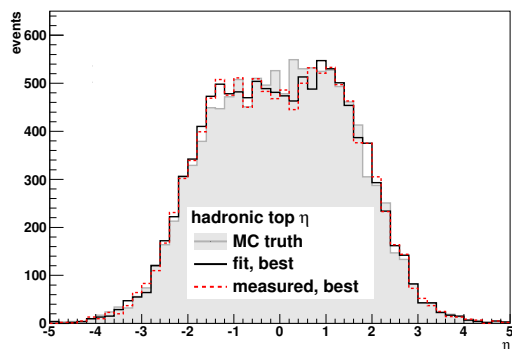
Also in the hadronic top p_T distributions no significant difference between the e +jets and μ +jets sample can be observed.



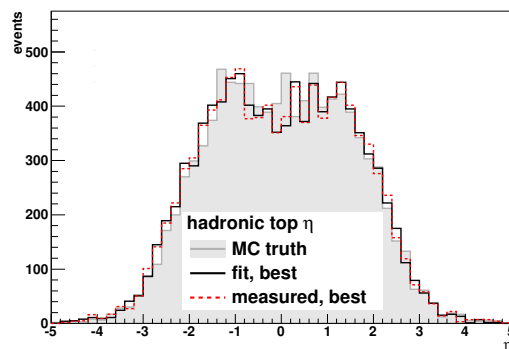
(a) μ +jets sample with free top mass



(b) e +jets sample with free top mass



(c) μ +jets sample with fixed top mass



(d) e +jets sample with fixed top mass

Figure A.3.: Comparison of e +jets and μ +jets with hadronic top η distribution.

These “hadronic” plots are qualitatively the same as the “leptonic” plots already discussed, but the discussed “dip” is not as distinctive in the “hadronic” plots.

B. Cuts on Wjets Sample

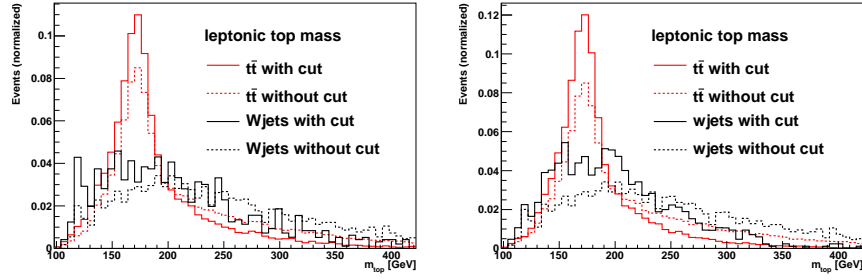
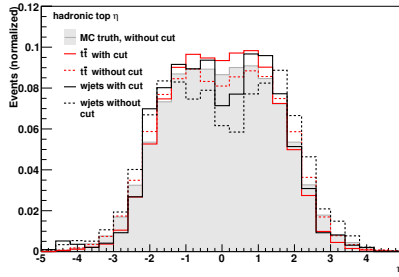
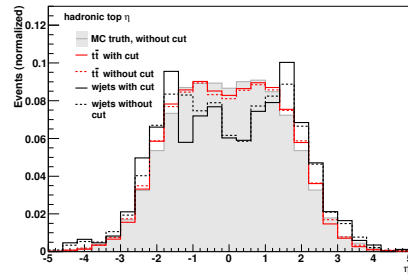
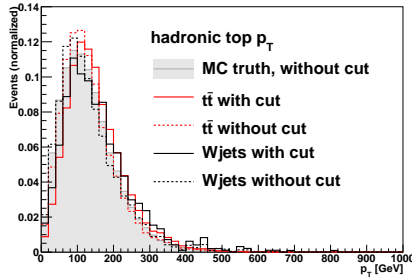
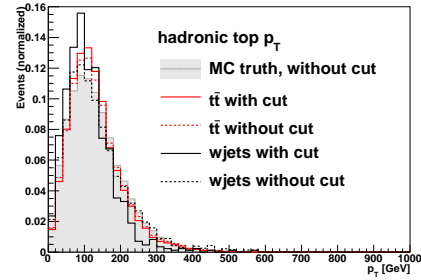
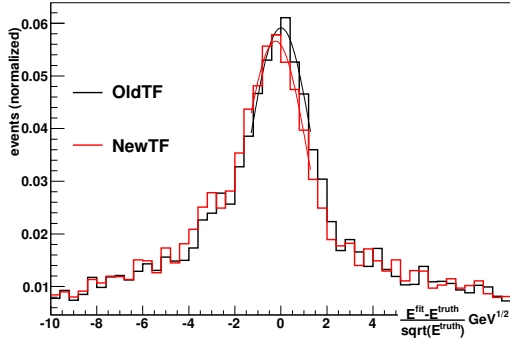
(a) leptonic top mass with and without ΔR cut(b) leptonic top mass with and without $\log L$ cut(c) hadronic top η with and without ΔR cut(d) hadronic top η with and without $\log L$ cut(e) hadronic top p_T with and without ΔR cut(f) hadronic top p_T with and without $\log L$ cut

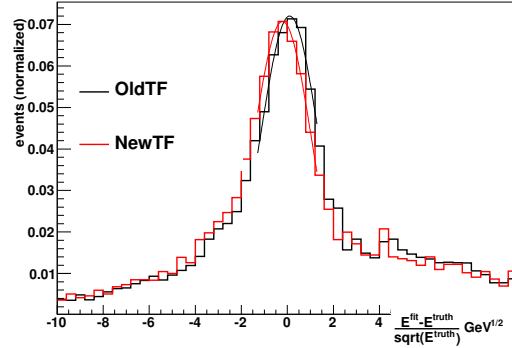
Figure B.4.: Selected distributions of signal (ejets) and background (wjets) with and without cut.

Regarding the top mass, the same things as discussed in Chapter 6.4.3 can be said. In the p_T distribution, the shift for the ΔR cut can also be observed. The wjets and signal distributions fit the hadronic η -distributions also better after both cuts, just like for the leptonic η -distributions already discussed.

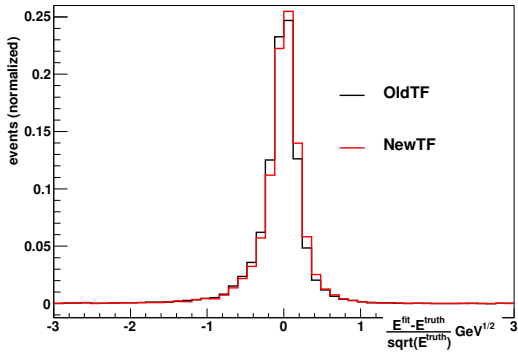
C. Comparison of two Sets of Transfer Functions on $e+jets$ Sample



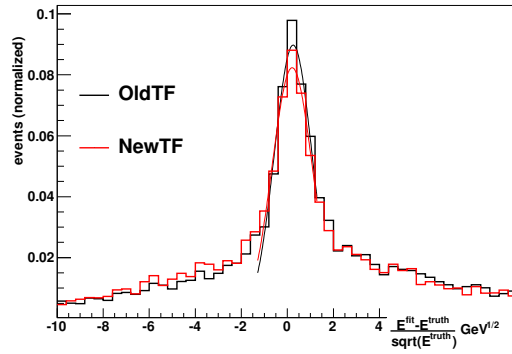
(a) hadronic b quark



(b) leptonic b quark



(c) electron



(d) energy resolution of the sum of the energy of both light quarks

Figure C.5.: Energy resolution of quarks and electron for the $e+jets$ sample.

The energy resolutions for the electron-sample behave like the energy resolutions for the muon-sample. But the energy resolution of the lepton (here of course the electron) is much broader than for the lepton (muon) in the muon-sample.

9. Appendix

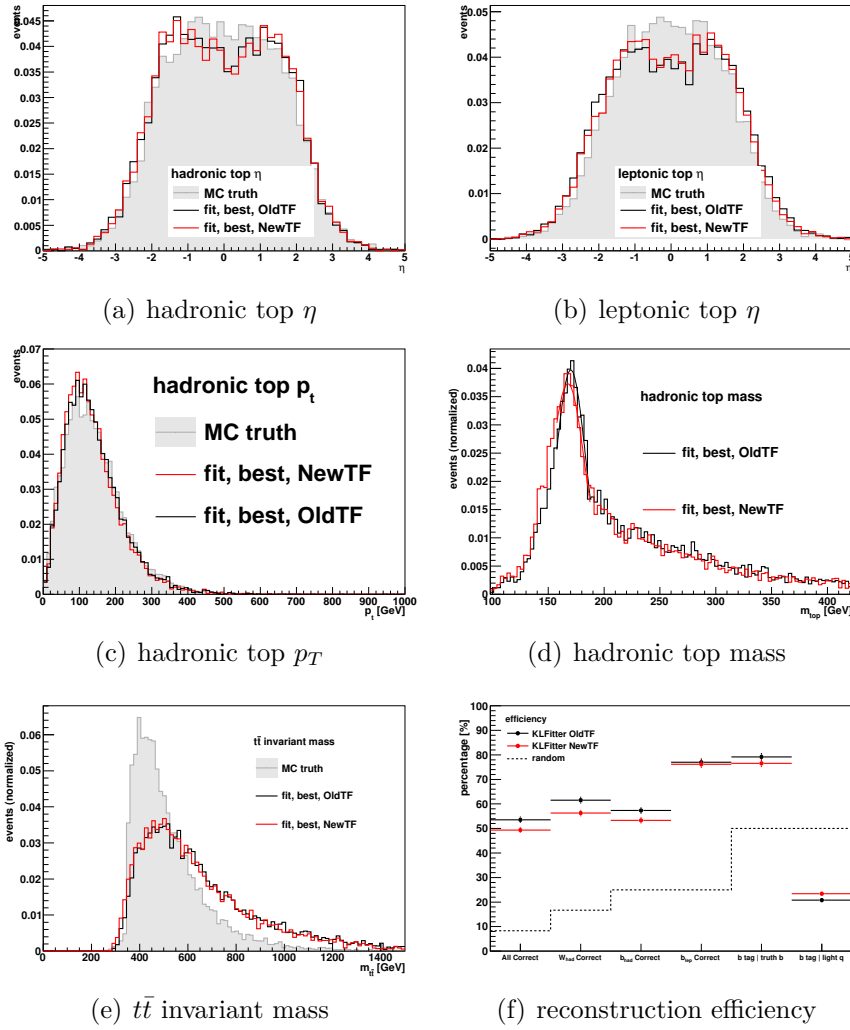


Figure C.6.: Comparison of both sets of transfer functions (NewTF and OldTF) for the ejets sample.

In the η -distribution no significant performance difference over the whole η -range of both sets of transfer functions can be observed. As for the muon-sample, in the electron-sample the efficiencies decrease with the NewTF-set and the peak of the top mass shifts to lower values.

Bibliography

- [1] D. Griffiths, *Introduction to Elementary Particles*, Wiley-VCH, 1987.
- [2] C. Berger, *Elementarteilchenphysik*, Springer, 2006.
- [3] B. Povh, K. Rith, C. Scholz, and F. Zetsche, *Teilchen und Kerne*, Springer, 1999.
- [4] C. Amster *et al.*, *Particle Physics Booklet*, Physics Letters **B**, 667 (2008).
- [5] F. Halzen and A. Martin, *Quarks & Leptons*, John Wiley & Sons, 1984.
- [6] N. Cabibbo, *Unitary Symmetry and Lepton Decays*, Physical Review Letters **10**, 531 (1963).
- [7] D. H. Perkins, *Introduction to High Energy Physics*, Cambridge University Press, 2000.
- [8] D0 collaboration, *Observation of the top quark*, Physical Review Letters **74**, 2632 (1995).
- [9] CDF collaboration, *Observation of top quark production in $\bar{p}p$ collisions*, Physical Review Letters **74**, 2626 (1995).
- [10] Tevatron Electroweak Working Group, *Combination of CDF and D0 Results on the Mass of the Top Quark*, arXiv **0903.2503** (2009).
- [11] A. Quadt, *Top quark physics at hadron colliders*, The European Physical Journal C - Particles and Fields **48**, 835 (2006), 10.1140/epjc/s2006-02631-6.
- [12] W. Bernreuther, *Top-quark physics at the LHC*, Journal of Physics G: Nuclear and Particle Physics **35**, 1 (2008).
- [13] ATLAS Collaboration, *The ATLAS Experiment at the CERN Large Hadron Collider*, Journal of Instrumentation **3**, S08003 (2008).

Bibliography

- [14] L. Lyons, *Statistics for nuclear and particle physicists*, Cambridge University Press, 1986.
- [15] R. J. Barlow, *Statistics – A Guide to the Use of Statistical Methods in the Physical Sciences*, John Wiley & Sons, 1989.
- [16] J. Erdmann, K. Kröninger, O. Nackenhorst, and A. Quadt, *Kinematic fitting of $t\bar{t}$ events using a likelihood approach – The KLFitter package*, ATLAS note ATL-COM-PHYS-2009-551 (2009).
- [17] R. Brun and F. Rademakers, *ROOT – An Object Oriented Data Analysis Framework*, Nuclear Instruments and Methods in Physics Research Section A **389**, 81 (1997).
- [18] A. Caldwell, D. Kollar, and K. Kröninger, *BAT - The Bayesian Analysis Toolkit*, Computer Physics Communications **180**, 2197 (2009).
- [19] S. Frixione and B. Webber, *Matching NLO QCD computations and parton shower simulations*, Journal of High Energy Physics **02**, 029 (2002).
- [20] G. Corcella *et al.*, *HERWIG 6: an eventgenerator for Hadron Emission Reactions With Interfering Gluons*, Journal of High Energy Physics **01**, 010 (2001).
- [21] O. Nackenhorst, *Top Quark Pair Reconstruction in the Electron + Jets Channel with a Kinematic Likelihood Fitter in the ATLAS Experiment*, Diploma thesis, Göttingen: II.Physik-UniGö-Dipl-2010/04 (2010).

Acknowledgements

First of all I would like to thank Johannes Erdmann for his intense supervision of my bachelor thesis. Even when he stayed in Paris, I could contact him via email and he always answered immediately to my questions. I highly appreciate that he spent so much time in proof-reading the fragments of my thesis. Moreover, I would like to thank Dr. Kevin Kröniger for his support of my thesis, for answering the enquiries concerning my work in the top meeting and for proof-reading my bachelor thesis. Sincere thank to Prof. Dr. Arnulf Quadt for giving me the opportunity of writing my bachelor thesis in the field of particle physics and for being the first referee of my thesis. Furthermore, I would like to thank Prof. Dr. Ariane Frey for being the second referee. Knowing full well that I am not the only student writing my bachelor thesis in the II. Institute of Physics, accept this token of my esteem for investing so much time, the more as a bachelor student knows virtually nothing about particle physics before he starts his thesis (at least I was in such a manner).

Erklärung nach §13(8) der Prüfungsordnung für den Bachelor-Studiengang Physik und den Master-Studiengang Physik an der Universität Göttingen:

Hiermit erkläre ich, dass ich diese Abschlussarbeit selbständig verfasst habe, keine anderen als die angegebenen Quellen und Hilfsmittel benutzt habe und alle Stellen, die wörtlich oder sinngemäß aus veröffentlichten Schriften entnommen wurden, als solche kenntlich gemacht habe.

Darüberhinaus erkläre ich, dass diese Abschlussarbeit nicht, auch nicht auszugsweise, im Rahmen einer nichtbestanden Prüfung an dieser oder einer anderen Hochschule eingereicht wurde.

Göttingen, den November 29, 2010

(Sven Ebert)